SYNTHESIS OF COPPER SULFIDE NANOPARTICLES

MISS JENJIRA SUWANJARUS

MR. WIROON TANGWIJITSAKUL

MISS SARITA WEERAKUL

A SPECIAL PROJECT SUBMITTED IN PARTIAL FULFILLMENT OF THE

REQUIREMENTS FOR THE DEGREE OF BACHELOR OF SCIENCE

IN PETROCHEMICAL TECHNOLOGY (INTERNATIONAL PROGRAMS)

FACULTY OF SCIENCE

KING MONGKUT'S INSTITUTE OF TECHNOLOGY LADKRABANG

2009

Spetial Project Title	Synthesis of copper sulfide nanoparticles
Student Names	Miss jenjira Suwanjarus
	Mr. Wiroon Tangwijitsakul
	Miss Sarita Weerakul
Degree	Bachelor of Science
Program	Petrochemical Technology (International Program)
Academic Year	2009
Advisor	Asst. Prof. Dr Pachernchaiyapat Chaiyasith

ABSTRACT

Copper Sulfide nanoparticle was synthesized using wet chemical method and emulsion liquid membrane. The effects of method used, temperature and mole ratio were studied. Products were characterized and analyzed by XRD, XRF, SEM and TEM techniques. All conditions giving result in rod-shaped copper sulfide nanoparticle which particle size are in range of 5 nm – 29 nm. The crystallinity is affected by synthesized method, the emulsion liquid membrane give higher crystallinity particles. The temperatures were set at 30°C, 60°C and 90°C which is resulting in the higher temperature, the larger the width of rods and the rounder shape. Mole ratio of Cu^{2+}:S^{2-} was varied at 1:1 and 2:1, the mole ratio 2:1 resulted in larger particle sized. The percent yield of product also observed, there are no significantly effects from any conditions and method.

Acknowledgement

The preparation of this project would not have been possible without the full support, hard work and endless efforts of a large number of individuals and institutions. We wish to express our gratitude to our supervisor; Asst. Prof. Pachernchaiyapat Chaiyasith who was abundantly helpful and offered invaluable assistance, support and guidance. Deepest gratitude is also due to the members of the supervisory committee, if without whose knowledge and assistance this study would not have been successful. We would also like to convey thanks to the Institution and Faculty of Science for providing the financial means and laboratory facilities. We are particularly grateful for the Project Implementation Staff lead by Coordinator, Team and Support instrumental in facilitating the work of all in particular; Instrumental science center, Faculty of Science, King Mongkut's institute of Technology Ladkrabang, Microscopic Center, Faculty of Science, Burapha University and Center of Nanoimaging (CNI), Mahidol University

Special thanks also to all our graduate friends, our senior, here in International program for their sharing the literature, encouragement and invaluable assistance. Not forgetting to our best friends who always been there.

Last and most of all, we wish to express our love and gratitude to our beloved families; for their understanding, encouragement, endless love, and constant support through the duration of our studies.

Miss jenjira Suwanjarus

Mr. Wiroon Tangwijitsakul

Miss Sarita Weerakul

Table of Contents

List of Tables

List of Figures

Chapter 1

Introduction

1.1 Rationale

Nanotechnology is the creation of new materials, devices, and systems through the control of matter on the nanometer-length scale, at the level of atoms and molecules. The essence of nanotechnology is the ability to work at these levels to generate nanostructures with fundamentally new molecular organization. Nanoparticles exhibit many unique properties, for which they are intensely being studied in a number of research fields. For example, they have very high surface area to volume ratio compared to bulk material. Nanoparticles can also enhance strength and uniformity of composite materials. Lastly, they show quantum confinement effects that form the basis in developing high technology devices. Several techniques have been developed for nanoparticles, some based on physical principle and some based on chemical principle. Used mechanical grinding as a means to attain nanoscale particles (<100 nm) is not practical for various reasons:

- The grain distribution is large
- Obtaining particles smaller than 1 μm is usually difficult
- The shape is irregular due to non-directed cracking
- Particle size distribution is board and uncontrolled

Therefore the need for procedure based on chemical principle is important. These procedures have been found to be promising due to their low energy requirements and better controller the particle size. However, in construction of photovoltaic device, nano-sized particles of n-type and p-type semiconducting materials and low bandgap semiconductors are necessary to

obtain the necessary absorption. Copper sulfide has suitable bandgap for semiconductor, so synthesize of copper sulfide nanoparticles is useful for photovoltaic industry.

Copper Sulfide is particular interest to the industry as it exhibits a metal-like electrical conductivity and semiconductor material. Furthermore it is also an importance material which processes nearly ideal solar control characteristics in part of energy [1,29] and widely applied in thin film and composite materials for their unique properties such as optoelectronic, high capacitance, catalytic, medicine, high speed computing systems, gas sensing, ink-jet printing technology and other branches of industry [2,32]. Based on these studies, there are the many methods for synthesis CuS nanoparticles such as electrospining, micro-emulsion, Langmuir-Blodgett films, solid state reaction, wet chemical, and emulsion liquid membrane etc. [30-31]

In this special project, the wet chemical method and Emulsion Liquid Membrane method are used to synthesize CuS nanoparticles. The effects of the synthesized method, concentration and temperature on the morphology, particle size and percent yield of CuS nanoparticles are investigated.

1.2 Objectives

1.2.1 To prepare copper sulfide nanoparticles using Wet Chemical Method and Emulsion Liquid Membrane

1.2.2 To obtain the suitable method for the preparation of copper sulfide nanoparticles

1.3 Scope of Study

1.3.1 Prepare Copper Sulfide Nanoparticles via

- Wet Chemical Method and
- Emulsion Liquid Membrane

Under following condition;

Mole ratio of Cu^{2+}:S^{2-} at 1:1 and 2:1,

Temperature at room temperature (30°C), 60°C and 90°C

1.3.2 Characterize the particles by using

- X-ray Diffraction: XRD
- X-ray Fluorescence: XRF
- Scanning Electron Microscope: SEM
- Transmission Electron microscopy: TEM

1.4 Expected Result

1.4.1 To prepare Copper sulfide particles in nano-range

Chapter 2

Theory and Related Literature

Part I. Material

2.1 Nanoparticles

In nanotechnology, a particle is defined as a small object that behaves as a whole unit in terms of its transport and properties. It is further classified according to size: In terms of diameter, fine particles cover a range between 100 and 2500 nanometers, while ultrafine particles are sized between 1 and 100 nanometers. Similarly to ultrafine particles, nanoparticles are sized between 1 and 100 nanometers. Nanoparticles may or may not exhibit size-related properties that differ significantly from those observed in fine particles or bulk materials. Although the size of most molecules would fit into the above outline, individual molecules are usually not referred to as nanoparticles.

Nanoclusters have at least one dimension between 1 and 10 nanometers and a narrow size distribution. Nanopowders are agglomerates of ultrafine particles, nanoparticles, or nanoclusters. Nanometer sized single crystals, or single-domain ultrafine particles, are often referred to as nanocrystals. Nanoparticle research is currently an area of intense scientific research, due to a wide variety of potential applications in biomedical, optical, and electronic fields.

Nanoparticles are of great scientific interest as they are effectively a bridge between bulk materials and atomic or molecular structures. A bulk material should have constant physical properties regardless of its size, but at the nano-scale this is often not the case. Size-dependent properties are observed such as quantum confinement in semiconductor particles, surface plasmon resonance in some metal particles and super paramagnetism in magnetic materials.

The properties of materials change as their size approaches the nanoscale and as the percentage of atoms at the surface of a material becomes significant. For bulk materials larger than one micrometer the percentage of atoms at the surface is minuscule relative to the total number of atoms of the material. The interesting and sometimes unexpected properties of nanoparticles are partly due to the aspects of the surface of the material dominating the properties in lieu of the bulk properties.

Nanoparticles exhibit a number of special properties relative to bulk material. For example, the bending of bulk copper (wire, ribbon, etc.) occurs with movement of copper atoms/clusters at about the 50 nm scale. Copper nanoparticles smaller than 50 nm are considered super hard materials that do not exhibit the same malleability and ductility as bulk copper. The change in properties is not always desirable. Ferroelectric materials smaller than 10 nm can switch their magnetization direction using room temperature thermal energy, thus making them useless for memory storage. Suspensions of nanoparticles are possible because the interaction of the particle surface with the solvent is strong enough to overcome differences in density, which usually result in a material either sinking or floating in a liquid. Nanoparticles often have unexpected visible properties because they are small enough to confine their electrons and produce quantum effects.

Nanoparticles have a very high surface area to volume ratio. This provides a tremendous driving force for diffusion, especially at elevated temperatures. Sintering can take place at lower temperatures, over shorter time scales than for larger particles. This theoretically does not affect the density of the final product, though flow difficulties and the tendency of nanoparticles to agglomerate complicates matters. The large surface area to volume ratio also reduces the incipient melting temperature of nanoparticles.

Moreover nanoparticles have been found to impart some extra properties to various day to day products. Like the presence of titanium dioxide nanoparticles impart what we call as the self-cleaning effect, and the size being nanorange, the particles can't be seen. Nano Zinc Oxide particles have been found to have superior UV blocking properties compared to its bulk substitute. This is one of the reasons why it is often used in the sunscreen lotions. Clay

nanoparticles when incorporated into polymer matrices increase reinforcement, leading to stronger plastics, verified by a higher glass transition temperature and other mechanical property tests. These nanoparticles are hard, and impart their properties to the polymer (plastic). Nanoparticles have also been attached to textile fibers in order to create smart and functional clothing [8].

Therefore, much attention has been paid to the application of nanoparticles. The reasons is that nanoparticles have some special properties, such as low melting point, low density and high surface area [10], which cannot be obtained from the macoparticles. In addition, interesting on the properties of a materials that can vary between the bulk and molecular scales also have attracted a great deal of attention due to the facts that many properties of the nanostructure materials are no longer follow the classical mechanic rules but instead can be explained in terms of the quantum mechanics [11].

2.2 Copper Sulfide

Copper monosulfide is a chemical compound of copper and sulfur. It occurs in nature as the dark indigo blue mineral covellite [5]. Its crystal structures consist of isolated sulfide anions that are closely related to lattices, without any direct S-S bonds. The copper ions are distributed in a complicated manner over interstitial sites with both trigonal as well as distorted tetrahedral coordination and are rather mobile. Therefore, this group of copper sulfides shows ionic conductivity at slightly elevated temperatures. In addition, the majority of its members are semiconductors [6].

Copper monosulfide crystallizes in the hexagonal crystal system, and this is the form of the mineral covellite. There is also an amorphous high pressure form, which has been described as having a distorted covellite structure. An amorphous room temperature semiconducting form, which is transforms to the crystalline covellite form at 30 °C [5].

The crystal structure of covellite has been reported several times, and whilst these studies are in general agreement on assigning the space group $P6_3/mmc$, there are small discrepancies in bond lengths and angles between them. The structure was described as "extraordinary" by Wells and is quite different from copper (II) oxide, but similar to CuSe (klockmannite). The covellite unit cell contains 6 formula units (12 atoms) in which [5]:

- 4 Cu atoms have tetrahedral coordination
- 2 Cu atoms have trigonal planar coordination
- 2 pairs of S atoms are only 207.1 pm apart indicating the existence of an S-S bond (a disulfide unit)
- The 2 remaining S atoms form trigonal planar triangles around the copper atoms, and are surrounded by five Cu atoms in a pentagonal bipyramid
- The S atoms at each end of a disulfide unit are tetrahedrally coordinated to 3 tetrahedrally coordinated Cu atoms and the other S atom in the disulfide

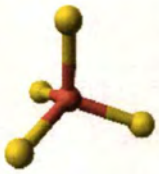

Tetrahedral coordination of copper

Trigonal planar coordination of copper

Trigonal bipyramidal coordination of sulfur

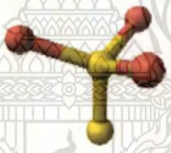

Tetrahedral coordination of sulfur-note disulfide unit

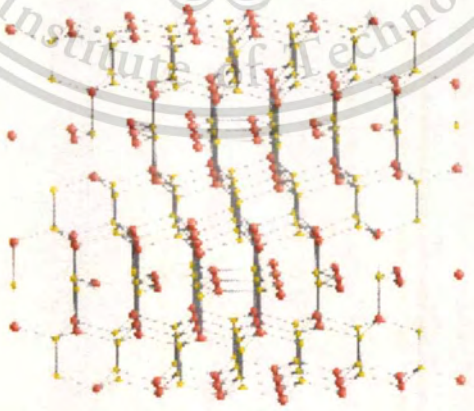

Ball-and-stick model of part of the crystal structure of covellite

Figure 2.1: The crystal structure of Copper and Sulfide

2.2.1 Covellite mineral information and data

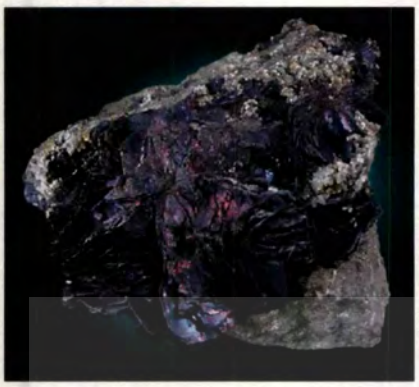

Covellite is usually as indigo-blue massive metallic material, sometimes with crystals on exposed surfaces. Good crystals extremely rare.

Figure 2.2: Show Covellite photo

IUPAC name: Copper sulfide

Other name: Cupric sulfide; Copper sulfide; CuS; C.I. Pigment Blue 34; C.I. 77450; Copper monosulfide; Copper sulfide (CuS); Copper Blue; Copper (II) sulfide; Horace Vernet's Blue; Oil Blue; Monocopper monosulfide

2.2.1.1 Crystallography

Crystal system: Hexagonal

Class (H-M): 6/*mmm (6/m 2/m 2/m)* - Dihexagonal Dipyramidal

Space group: $P6_3/mmc$ *{*$P6_3/m$ *2/m 2/c}*

Cell parameters: a = 3.7938Å, c = 16.341Å

Ratio: a:c = 1 : 4.307

Unit cell volume: V 203.7 Å^3

Z: 6

Morphology: Hexagonal plates {001}, with pyramidal faces striated horizontally and hexagonal striations on the base. Common forms: {001}, {104}, {103}, {308}, {102}, {9/0/16}, {5.08}, {101} and {201}. Less common to rare: {1.0.16}, {1.0.12}, {3.0.32}, {108}, {106}, {3.0.16}, {105}, {205}, {203}, {304}, {15.0.16} and {908}.

2.2.1.2 Physical properties

Color: Indigo-blue or darker, inclining towards blue-black, often iridescent with purplish, deep red, and brassy-yellow reflections.

Luster: Sub-metallic

Diaphaneity: Opaque

Streak: Shiny metallic, lead-grey to black

Hardness: 1.5 - 2 Mohs

VHN_{100}=128 - 138 kg/mm^2 (Vickers)

Tenacity: Flexible

Cleavage: Perfect on {0001}

Fracture: Brittle - Generally displayed by glasses and most non-metallic minerals.

Density: 4.6 - 4.76 g/cm^3 (Measured)

4.602 g/cm^3 (Calculated)

2.2.1.3 Chemical properties

Formula: CuS

Essential elements: Cu, S

All elements listed in formula: Cu, S

Analytical data: Wet chemical analysis of ideal material given

Cu 66.47

S 33.53

Total 100.00

Empirical formula: $Cu_{0.99}S_{1.00}$

Common impurities: Fe, Se, Ag, Pb

2.2.1.4 Calculated properties

Electron density: Bulk Density (Electron Density) = 4.41 gm/cc

note: Specific Gravity of Covellite = 4.68 gm/cc.

Fermion Index: Fermion Index = 0.0025153223

Boson Index = 0.9974846777

Photoelectric: $PE_{Covellite}$ = 31.55 barns/electron

$U=PE_{Covellite}$ x rElectron Density= 139.00 barns/cc.

Radioactivity: GRapi = 0 (Gamma Ray American Petroleum Institute Units)

Covellite is Not Radioactive

2.2.1.5 Optical Data

Type: Uniaxial (+), w=1.45, e=2.62, bire=1.1700.

RI values: $n_\omega = 1.450$ $n_\varepsilon = 2.620$

Maximum Birefringence:

$\delta = 1.170$

Chart shows birefringence interference colour range (at 30μm thickness) and does not take into account mineral coloration.

2.2.1.6 X-ray powder diffraction

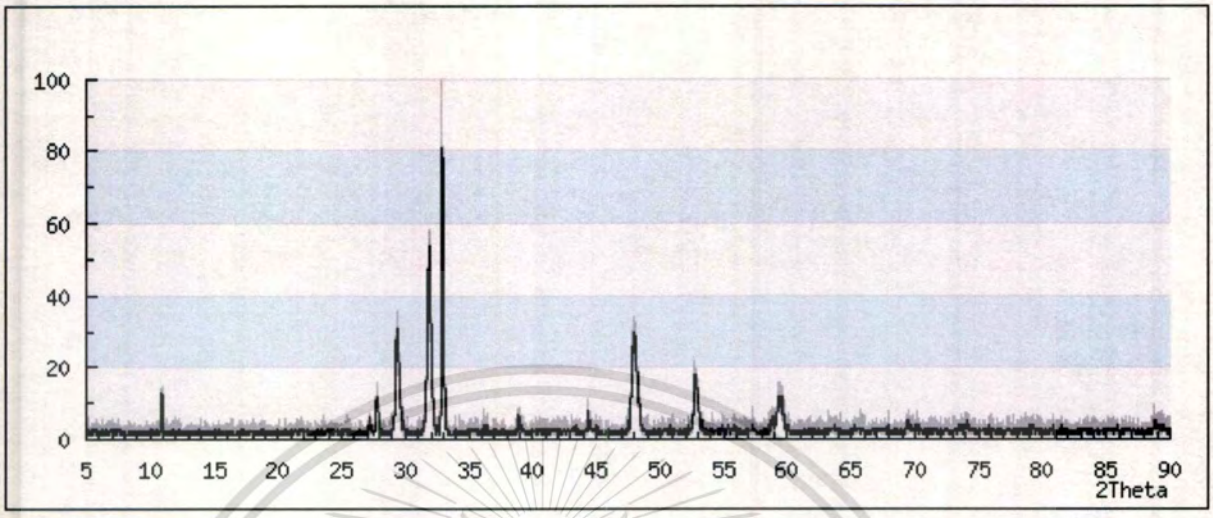

Figure 2.3: The X-ray Diffraction of CuS

Radiation - Copper Kα

Data Set: Butt, Montana, USA

Horizontal axis: 5° to 90°

Vertical axis: 100%

Data courtesy of RRUFF project at University of Arizona, used with permission.

Part II. Synthesis Method

2.3 Copper Sulfide nanoparticle preparation

Copper sulfide is an important based material as absorber coating and is widely used in photovoltaic and photodetectors applications (due to its unique near solar control characteristics), IR detectors, optical filters, super ionic materials and can be used as additive in lubricating grease and filter in polymer to increase the tribological behavior.

2.3.1 Related literature

There are various reported methods for synthesizing CuS materials;

- Santosh et al. 1995 [16] synthesized CuS using reaction of copper ammonia complex with an equimolar thiourea solution in Triton-X 100/cyclohexane water-in-oil micro emulsions
- Reavskaya et al. 2003 [17] synthesized CuS colloidal nanoparticles using an indirect synthesis of CuS from CdS nanoparticles
- Kaibin et al. 2003 [15] synthesized special morphologies, such as flower- and trepan-like morphology, of CuS via a simple solution route at low temperature from CuO crystals.
- Mousa et al. 2005 [18] study in to the precipitation of CuS and ZnS in a semi-batch-wise operated bubble column
- Ujjal and Bratindranath 2005 [12] prepared water-soluble CuS nanocrystals and nanorods by reaction of copper acetate and thioacetamide in the presence of different surfactants and capping agents. The size of the nanocrystals varied from 3-20 nm.
- Chunyan et al. 2006 [19] synthesized CuS nanotubes of 30-90 nm in inner diameter and 25-50 nm in thickness by a facike solution reaction at 80°C in ethylene glycol using Cu nanowires as templates and suitable sulfur sources for sulfuratuion reaction

- Poilomi and Suneel 2006 [20] synthesized CuS nanorods of length 60-100 nm and 15 nm in diameter by simples wet chemical method at 105°C using $CuCl_2.2H_2O$ as Cu-precursor, CS_2 as S-source and ethylendiamines as attacking reagent
- Keitaro et al. 2006 [21] developed a one-step, corrosion-assisted reaction to synthesized CuS from elemental copper and sulfur in water at 60°C. The prepared CuS consists of polyhedral-shaped 2-3 nm crystallites.
- Lihua et al. 2008 [22] developed a facile, ionic liquid-assisted route to synthesized hierarchical CuS flower-like sub-microspheres at 80°C for 24 hours. Resulted in floewery sphere with 0.6-1.0 micron and nanoflakes with a thickness of 10-20 nm.
- Ding et al. 2008 [23] prepared CuS hexagonal nanoplatelets by a simple hydrothermal process at mild temperature, using sodium dodecyl benzene sulfonate as an assisting reagent.
- Limei et al. 2009 [24] prepared CuS nanoparticles with mean diameter about 1 nm in copper bromide-based perovskite organic-inorganic crystal hybrid templates by reacting their spin-casting films with H_2S gas.

2.3.2 Preparation Methods

2.3.2.1 Wet Chemical Method

Wet chemical Methods including sol-gel co-precipitation, and hydrothermal synthesis were developed to obtain ultrafine, very homogeneous and new synthesis compositions which allow one to lower the sintering temperatures and to control the microstructure [7].

Copper sulfide precipitated via ionic reaction:

$$Cu^{2+}_{(aq)} + S^{2-}_{(aq)} \rightarrow CuS_{(s)}$$

2.3.2.2 Solid Reaction

Solid reaction or dry media reaction is a chemical reaction system in the absence of the solvent. The drive for the development of dry media reaction in chemistry is economics, ease of purification, high reaction rate and environmental friendly [9].

The modified solid reaction of CuS synthesized was reported by Keito et al. 2006 [21], water was added to the solid-state reaction in order to avoid the passivation of the reactive copper surface, with occur at the low temperature, non-aqueous solid-state reaction. The addition of water also freshened copper surface to react with sulfur and form CuS at low temperature.

$$Cu_{(s)} + S_{(s)} \rightarrow CuS_{(s)}$$

2.3.2.3 Emulsion Liquid Membrane

Emulsion Liquid membranes were first developed by Li at Exxon. Bubble or liquid emulsion membranes have a large number of applications in removal and recovery of metals from large, dilute solutions. In recent times, this method has been used for the synthesis of nanoparticles and macromolecular size particles. The use of internal phase to control particle size and morphology has been a recent point of interest.

The process consists of four main steps. The first step is mixing the aqueous internal phase with an organic phase to form a liquid/oil emulsion. It is then further mixed in a larger mixing vessel with an external aqueous phase to form a water/oil/water emulsion. The external phase contains the ions that will be transported across the membrane to react with the internal phase.

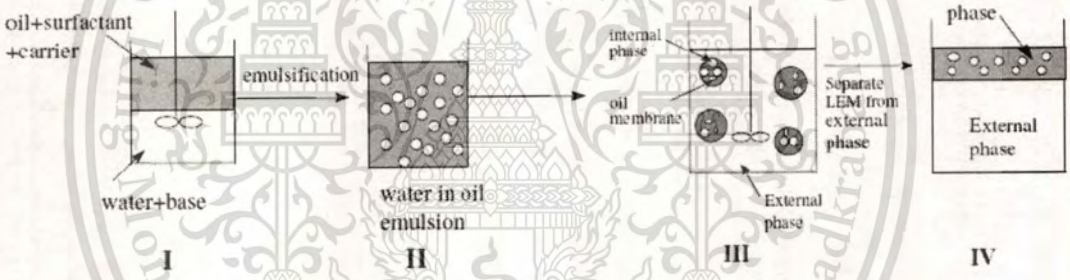

Figure 2.4: Show four main steps of Emulsion Liquid membranes

The transport of metal ions occurs via facilitated transport using carriers and concentration gradients from the feed solution though the walls of the emulsion into the product solution. This occurs in the third phase. Here the metal ions form precipitates which can then later be removed as product after the solution has been demulsified. The minute emulsion droplets are commonly referred to as micro reactors. The micro sized internal emulsion droplets are considered as separate reactors such that the control of particle size is independent of the overall solution conditions but that within the emulsion droplet [25].

In this work, Wet Chemical Method and Emulsion Liquid Membrane were used to synthesize CuS nanoparticle to compare the synthesized particles from each method.

Part III. Characterization Technique

2.4 X-Ray Diffraction Technique: XRD

X-ray Diffraction (XRD) is one of the techniques for qualitative and quantitative analysis of crystalline compounds. The technique provides information that cannot be obtained any other way. The information obtained includes types and nature of crystalline phases present, structural makeup of phases, degree of crystallinity, amount of amorphous content, microstrain and size and orientation of crystallites.

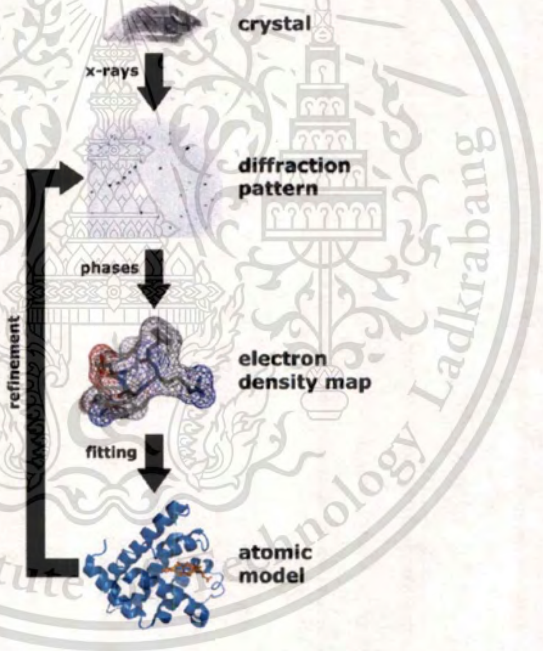

Figure 2.5: Workflow for solving the structure of a molecule by X-ray crystallography

X-ray diffraction techniques are based on the elastic scattering of x-rays from structures that have long range order. The most comprehensive description of scattering from crystals is given by the dynamical theory of diffraction. [33]

- Single-crystal X-ray diffraction is a technique used to solve the complete structure of crystalline materials, ranging from simple inorganic solids to complex macromolecules, such as proteins.
- Powder diffraction (XRD) is a technique used to characterize the crystallographic structure, crystallite size (grain size), and preferred orientation in polycrystalline or powdered solid samples. Powder diffraction is commonly used to identify unknown substances, by comparing diffraction data against a database maintained by the International Centre for Diffraction Data. It may also be used to characterize heterogeneous solid mixtures to determine relative abundance of crystalline compounds and, when coupled with lattice refinement techniques, such as Rietveld refinement, can provide structural information on unknown materials. Powder diffraction is also a common method for determining strains in crystalline materials.
- Thin film diffraction and grazing incidence x-ray diffraction may be used to characterize the crystallographic structure and preferred orientation of substrate-anchored thin films.
- High-resolution x-ray diffraction is used to characterize thickness, crystallographic structure, and strain in thin epitaxial films. It employs parallel-beam optics.
- X-ray pole figure analysis enables one to analyze and determine the distribution of crystalline orientations within a crystalline thin-film sample.
- X-ray rocking curve analysis is used to quantify grain size and mosaic spread in crystalline materials

2.4.1 Scherrer equation

The Scherrer equation is used to determine crystallite sizes from XRD spectra. They contain K, a shape factor, which varies from 0.89 for spherical to 0.94 for cubic particles. Usually, this is set to 0.9 for particles of unknown size.

A shape factor is used in x-ray diffraction and crystallography to correlate the size of sub-micrometer particles, or crystallites, in a solid to the broadening of a peak in a diffraction pattern. In the Scherrer equation,

$$t = \frac{K\lambda}{B\cos\theta}$$

where K is the shape factor, λ is the x-ray wavelength, typically 1.54 Å, B is the line broadening at half the maximum intensity (FWHM) in radians, and θ is the Bragg angle; t is the mean size of the ordered (crystalline) domains, which may be smaller or equal to the grain size. The dimensionless shape factor has a typical value of about 0.9, but varies with the actual shape of the crystallite. The Scherrer equation is limited to nano-scale particles. It is not applicable to grains larger than about 0.1 μm, which precludes those observed in most metallographic and ceramographic microstructures.

It is important to realize that the Scherrer formula provides a lower bound on the particle size. The reason for this is that a variety of factors can contribute to the width of a diffraction peak; besides particle size, the most important of these are usually inhomogeneous strain and instrumental effects. If all of these other contributions to the peak width were zero, then the peak width would be determined solely by the particle size and the Scherrer formula would apply. If the other contributions to the width are non-zero, then the particle size can be larger than that predicted by the Scherrer formula, with the "extra" peak width coming from the other factors. [34]

Sathish Sukumaran's Derivation of Scherrer Equation [35]

Bragg's law is given by,

$$\lambda = 2dsin\theta \quad (1)$$

Multiply both sides by an integer m such that md=t, the thickness of the crystal. This leads to,

$$m\lambda = 2mdsin\theta = 2tsin\theta \quad (2)$$

Eqn. (2) can also be interpreted as the mth order reflection from a set of planes with an interplanar distance t.

Differentiate both sides of eqn. (2) remembering mλ is a constant. This gives,

$$0 = 2\Delta tsin\theta + 2tcos\theta\Delta\theta \quad (3)$$

Remembering that as $\Delta\theta$ can be positive or negative (we are only interested in absolute values) leads to,

$$t = \frac{\Delta tsin\theta}{cos\theta\Delta\theta} \quad (4)$$

Since the smallest increment in t is d, using $\Delta t = d$, and substituting $\lambda/2$ for $dsin\theta$ (from Bragg's law) we get,

$$t = \frac{\lambda}{2cos\theta\Delta\theta} \quad (4)$$

Substituting B for $2\Delta\theta$, the angular width, we get,

$$t = \frac{\lambda}{Bcos\theta} \quad (5)$$

which is essentially Scherrer equation.

A more sophisticated analysis of the problem only adds a prefactor of 0.9 to the right hand side of eqn. (5) and leads to the correct Scherrer equation.

$$t = \frac{0.9\lambda}{Bcos\theta} \quad (6)$$

2.5 X-Ray fluorescence Technique: XRF [36]

X-ray Fluorescence (XRF) spectroscopy is a nondestructive technique for Quantitative analysis of small volumes of solid and liquid samples. XRF spectroscopy is measuring the intensity of x-ray emitted from a specimen as a function of energy of wavelength the energy of large intensity lines are characteristic of atoms of the specimen. The intensities of observed lines for a given atom vary as the amount of that atom present in the specimen.

XRF is the emission of characteristic "secondary" (or fluorescent) X-rays from a material that has been excited by bombarding with high-energy X-rays or gamma rays. The phenomenon is widely used for elemental analysis and chemical analysis, particularly in the investigation of metals, glass, ceramics and building materials, and for research in geochemistry, forensic science and archaeology.

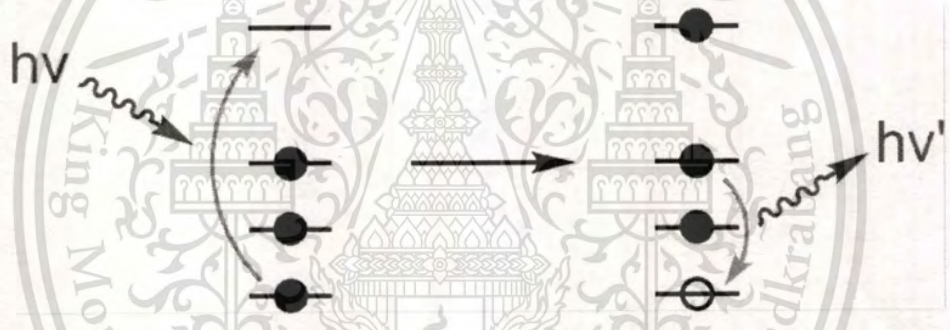

Figure 2.6: Physics of X-ray fluorescence, in a schematic representation.

The use of a primary X-ray beam to excite fluorescent radiation from the sample was first proposed by Glocker and Schreiber in 1928[1]. Today, the method is used as a non-destructive analytical technique, and as a process control tool in many extractive and processing industries. In principle, the lightest element that can be analyzed is beryllium (Z = 4), but due to instrumental limitations and low X-ray yields for the light elements, it is often difficult to quantify elements lighter than sodium (Z = 11), unless background corrections and very comprehensive interelement corrections are made.

2.5.1 Energy dispersive spectrometry

In energy dispersive spectrometers (EDX or EDS), the detector allows the determination of the energy of the photon when it is detected. Detectors historically have been based on silicon semiconductors, in the form of lithium-drifted silicon crystals, or high-purity silicon wafers.

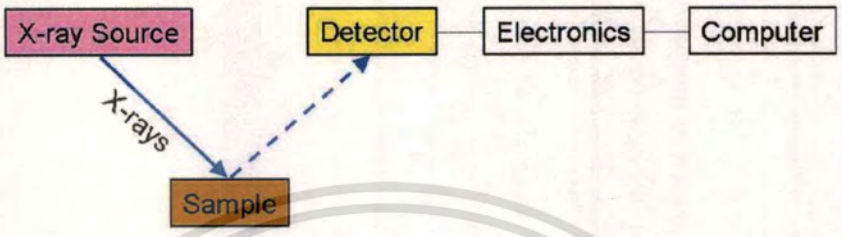

Figure 2.7: Schematic arrangement of EDX spectrometer.

2.5.2 Wavelength dispersive spectrometry

In wavelength dispersive spectrometers (WDX or WDS), the photons are separated by diffraction on a single crystal before being detected. Although wavelength dispersive spectrometers are occasionally used to scan a wide range of wavelengths, producing a spectrum plot as in EDS, they are usually set up to make measurements only at the wavelength of the emission lines of the elements of interest.

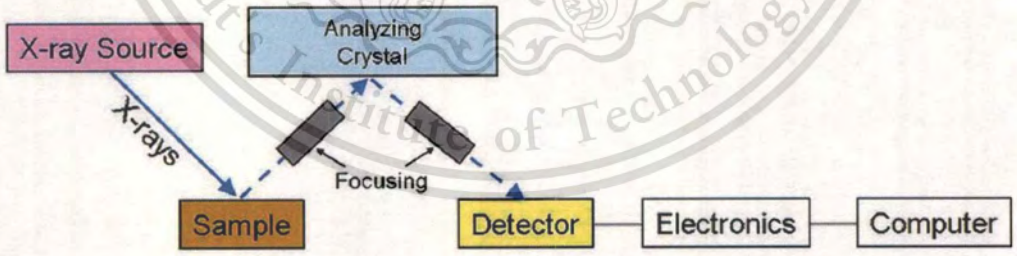

Figure 2.8: Schematic arrangement of wavelength dispersive spectrometer.

2.6 Scanning Electron microscopy: SEM [37]

Scanning Electron Microscope (SEM) is one of the techniques for surface characterization. SEM uses electrons to form images rather than light. SEM has several advantages including large depth of field, high image resolution or high magnification, relatively easy to prepare samples. SEM has a large of field, which allows a large area of sample surfaces to be in-focus at same time.

SEM is a type of electron microscope that images the sample surface by scanning it with a high-energy beam of electrons in a raster scan pattern. The electrons interact with the atoms that make up the sample producing signals that contain information about the sample's surface topography, composition and other properties such as electrical conductivity.

Figure 2.9: SEM opened sample chamber.

The types of signals produced by an SEM include secondary electrons, back-scattered electrons (BSE), characteristic X-rays, light (cathodoluminescence), specimen current and transmitted electrons. Secondary electron detectors are common in all SEMs, but it is rare that a single machine would have detectors for all possible signals. The signals result from interactions of the electron beam with atoms at or near the surface of the sample. In the most common or standard detection mode, secondary electron imaging or SEI, the SEM can produce very high-resolution images of a sample surface, revealing details about less than 1 to 5 nm in size. Due to the very narrow electron beam, SEM micrographs have a large depth of field yielding

a characteristic three-dimensional appearance useful for understanding the surface structure of a sample. This is exemplified by the micrograph of pollen shown to the right. A wide range of magnifications is possible, from about 10 times (about equivalent to that of a powerful hand-lens) to more than 500,000 times, about 250 times the magnification limit of the best light microscopes. Back-scattered electrons (BSE) are beam electrons that are reflected from the sample by elastic scattering. BSE are often used in analytical SEM along with the spectra made from the characteristic X-rays. Because the intensity of the BSE signal is strongly related to the atomic number (Z) of the specimen, BSE images can provide information about the distribution of different elements in the sample. For the same reason, BSE imaging can image colloidal gold immuno-labels of 5 or 10 nm diameter which would otherwise be difficult or impossible to detect in secondary electron images in biological specimens. Characteristic X-rays are emitted when the electron beam removes an inner shell electron from the sample, causing a higher energy electron to fill the shell and release energy. These characteristic X-rays are used to identify the composition and measure the abundance of elements in the sample.

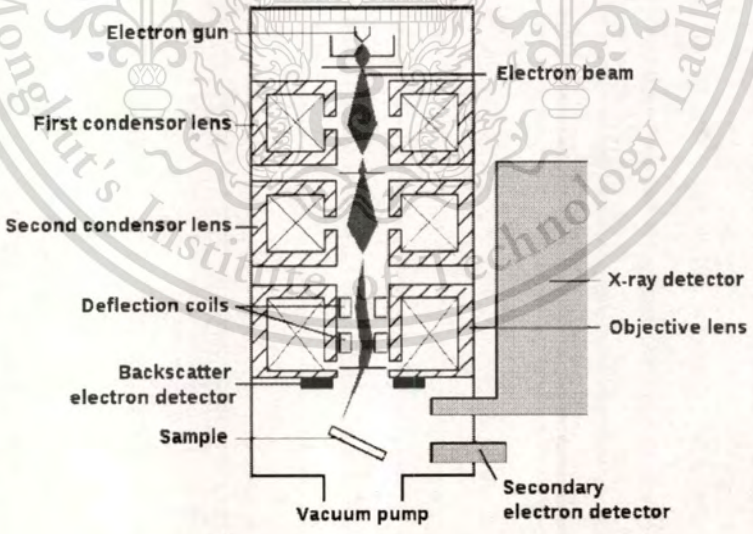

Figure 2.10: Schematic diagram of an SEM.

2.7 Transmission Electron Microscopy: TEM [38]

The Transmission Electron microscope allows the investigation of the internal microstructure of samples using electron as the source of illumination. In image mode, the objective lens produces an image of the internal structure of the specimen which is then projected and magnified, using a combination of projector and intermediate lenses, onto the fluorescent screen at the base of the column. Crystallographic information from the sample can be obtained by analysis of diffraction patterns when the TEM is operated in diffraction mode.

Figure 2.11: TEM machine, Philips, TECNAI 20

TEM is a microscopy technique whereby a beam of electrons is transmitted through an ultra thin specimen, interacting with the specimen as it passes through. An image is formed from the interaction of the electrons transmitted through the specimen; the image is magnified and focused onto an imaging device, such as a fluorescent screen, on a layer of photographic film, or to be detected by a sensor such as a CCD camera.

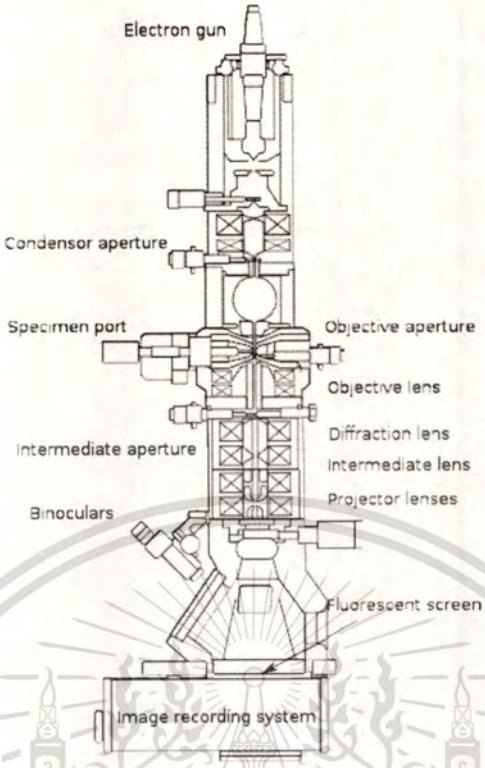

Figure 2.12: Layout of optical components in a basic TEM.

TEMs are capable of imaging at a significantly higher resolution than light microscopes, owing to the small de Broglie wavelength of electrons. This enables the instrument's user to examine fine detail—even as small as a single column of atoms, which is tens of thousands times smaller than the smallest resolvable object in a light microscope. TEM forms a major analysis method in a range of scientific fields, in both physical and biological sciences. TEMs find application in cancer research, virology, materials science as well as pollution and semiconductor research.

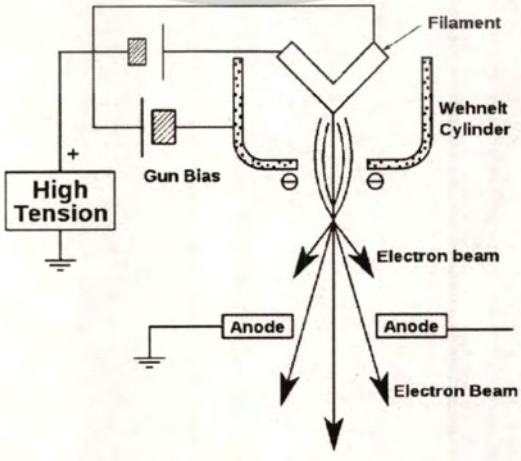

Figure 2.13: Cross sectional diagram of an electron gun assembly, illustrating electron extraction.

At smaller magnifications TEM image contrast is due to absorption of electrons in the material, due to the thickness and composition of the material. At higher magnifications complex wave interactions modulate the intensity of the image, requiring expert analysis of observed images. Alternate modes of use allow for the TEM to observe modulations in chemical identity, crystal orientation, electronic structure and sample induced electron phase shift as well as the regular absorption based imaging.

The first TEM was built by Max Knoll and Ernst Ruska in 1931, with this group developing the first TEM with resolving power greater than that of light in 1933 and the first commercial TEM in 1939.

Chapter 3

Experimental Procedure

3.1 Apparatus and Equipment

- Glassware
- Magnetic bars
- Heater and stirrer
- Vacuum filter set with pump
- Filter papers
- Digital balance
- Ultrasonic homogenizer
- Analytical Instruments
    - X-ray Diffraction (XRD); Bruker AXS, D8 ADVANCE
    - X-ray Fluorescence (XRF); Bruker AXS, SRS 3400
    - Scanning Electron Microscope (SEM)
    - Transmission Electron microscope (TEM); Philips, TECNAI 20

3.2 Chemicals

- Copper chloride: $CuCl_2 \cdot 2H_2O$ (Molecular weight = 170.47)
- Sodium sulfide: $Na_2S \cdot 9\ H_2O$ (Molecular weight = 240.18)
- Distilled water
- Kerosene (organic-phase)
- N-butanol (Demulsifier)
- Detergent, Sunlight Lemon Turbo ™

3.3 Experimental

3.3.1 Preparation of Copper Chloride and Sodium Sulfide Solutions

Mole ratio Cu^{2+}:S^{2-} , 1:1

- The Copper source solution was prepared by dissolving Copper(II) Chloride 21.31 g in distilled water into 250-mL volumetric flask to obtain 0.5 mol/L $CuCl_2$ solution
- The Sulfide source solution was prepared by dissolving Sodium Sulfide 30.02 g in distilled water into 250-mL volumetric flask to obtain 0.5 mol/L Na_2S solution

Mole ratio Cu^{2+}:S^{2-} , 2:1

- The Copper source solution was prepared by dissolving Copper(II) Chloride 42.62 g in distilled water into 250-mL volumetric flask to obtain 1.0 mol/L $CuCl_2$ solution
- The Sulfide source solution was prepared by dissolving Sodium Sulfide 30.02 g in distilled water into 250-mL volumetric flask to obtain 0.5 mol/L Na_2S solution

3.3.2 Preparation of Copper Sulfide Nanoparticles by Wet Chemical Method

- The solution comprises two types: Distilled water 150-mL was mixed without surfactant and with 0.1-mL detergent in the 600-mL beaker.
- The solution temperature was adjusted at room temperature (30°C), 60°C and 90°C, and then was stirred with magnetic stirrer. The equipment was connected as shown in Figure 3.1
- The Copper source solution ($CuCl_2$) 50-mL and Sulfide source solution (Na_2S) 50mL (in mole ratio of $Cu^{2+}:S^{2}$ = 1:1 and 2:1, respectively) were added into burettes. Then the both of them were dropped into the solution at flow rate = 1-mL/min.
- The precipitation will occur immediately

$$Cu^{2+}_{(aq)} + S^{2-}_{(aq)} \rightarrow CuS_{(s)}$$

- After 3 minutes from the last drop of solution, the stirrer was stopped, then the solution was cooled down to room temperature
- The CuS precipitates were collected and dried in oven at 60°C
- The samples were taken to characterize

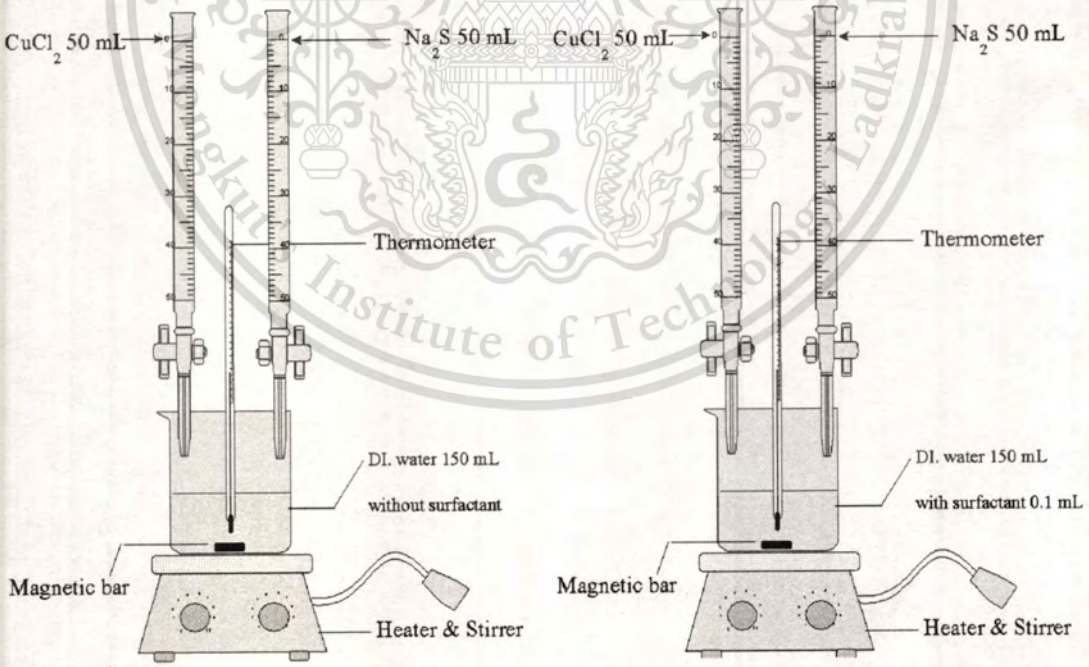

Figure 3.1: The equipment used for Wet Chemical Method.

Flow Diagram

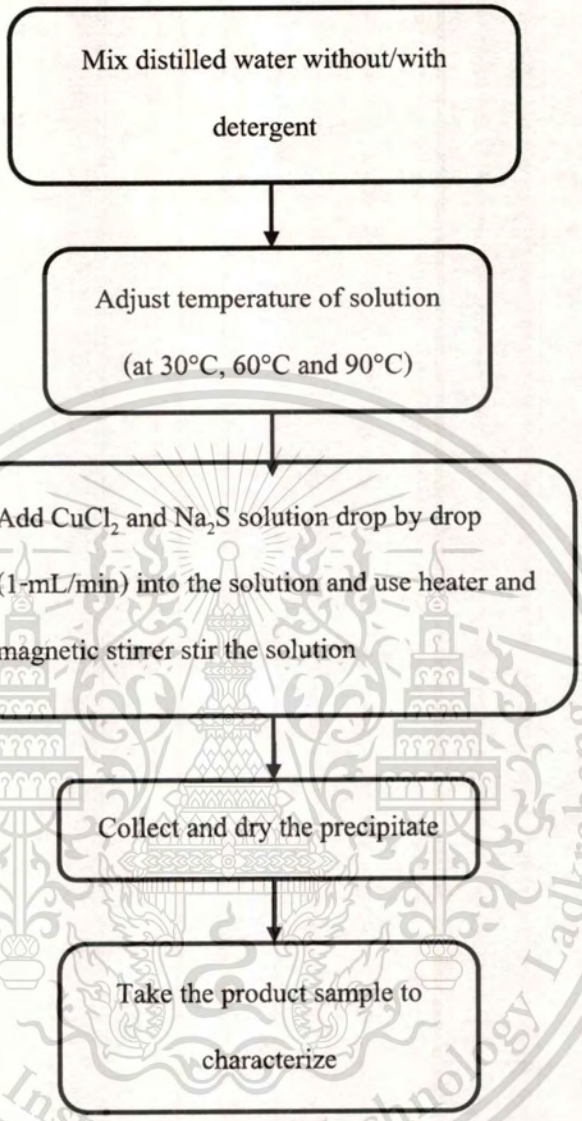

Figure 3.2: Flow diagram of Wet Chemical Method

3.3.3 Preparation of Copper Sulfide Nanoparticles by Emulsion Liquid Membrane

- The stripping phase was prepared by dissolving Sodium sulfide 30.02 g in distilled water into 250-mL volumetric flask
- The organic, membrane phase was prepared containing carrier and emulsifying agent (detergent 10.0-mL) on the basis by dissolving this reagent in kerosene 600-mL
- The 50-mL of the stripping phase and the organic membrane phase were mixed and emulsified by using magnetic stirrer as shown in figure 3.3
- The feed phase was prepared by dissolving copper chloride 21.31g in distilled water into 250-mL volumetric flask
- The Water-in-Oil emulsion was mixed with 250-mL DI water and stirred mechanically to obtain Water-in-Oil-in-Water emulsion
- The emulsion temperature was adjusted at room temperature (30°C), 60°C and 90°C
- The 50-mL of the feed phase was added into Water-in-Oil-in-Water emulsion 1mL/min drop by drop, in various molar 0.5M and 1.0M
- The precipitation will occur

$$Cu^{2+}_{(aq)} + S^{2-}_{(aq)} \rightarrow CuS_{(s)}$$

- The equipment was set as shown in figure 3.4
- After 3 minutes from the last drop of solution, the stirrer was stopped, then the emulsion was cooled down to room temperature
- The emulsion was transferred to separate the feed phase from the Water-in-Oil emulsion which contain the precipitates
- The Water-in-Oil emulsion was washed several times with water, then demulsified by adding n-butanol
- The organic phase was taken away
- The precipitate particles were filtered from stripping phase, washed thoroughly with water and n-butanol
- The product powders were dried and collected to characterize

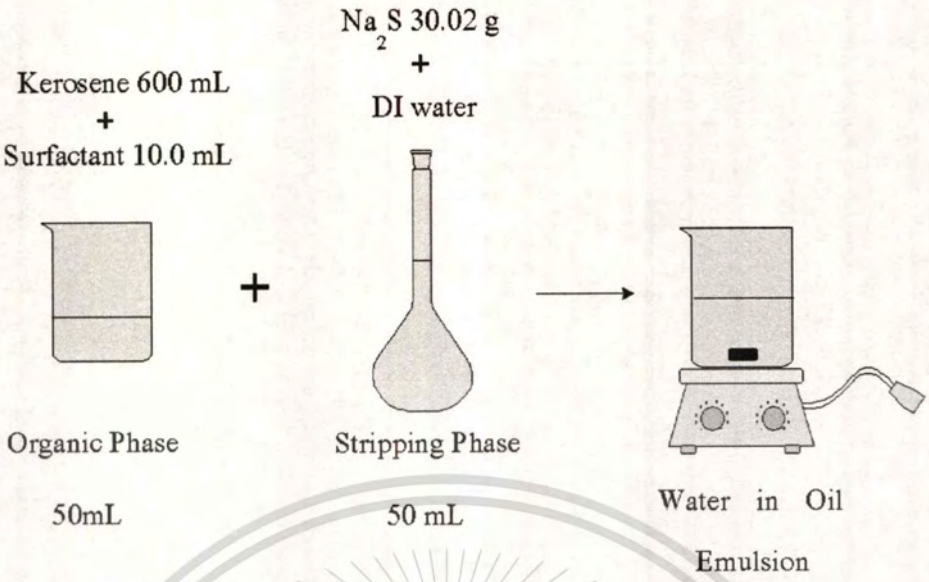

Figure 3.3: Preparation of water in oil emulsion

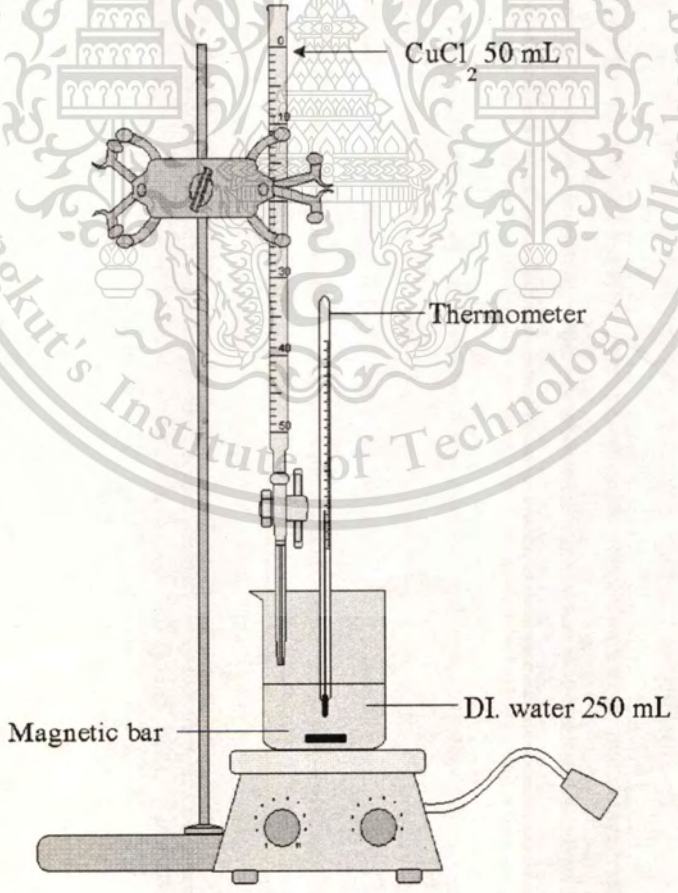

Water in Oil in Water Emulsion

Figure 3.4: The equipment used for Emulsion Liquid Membrane

Flow diagram

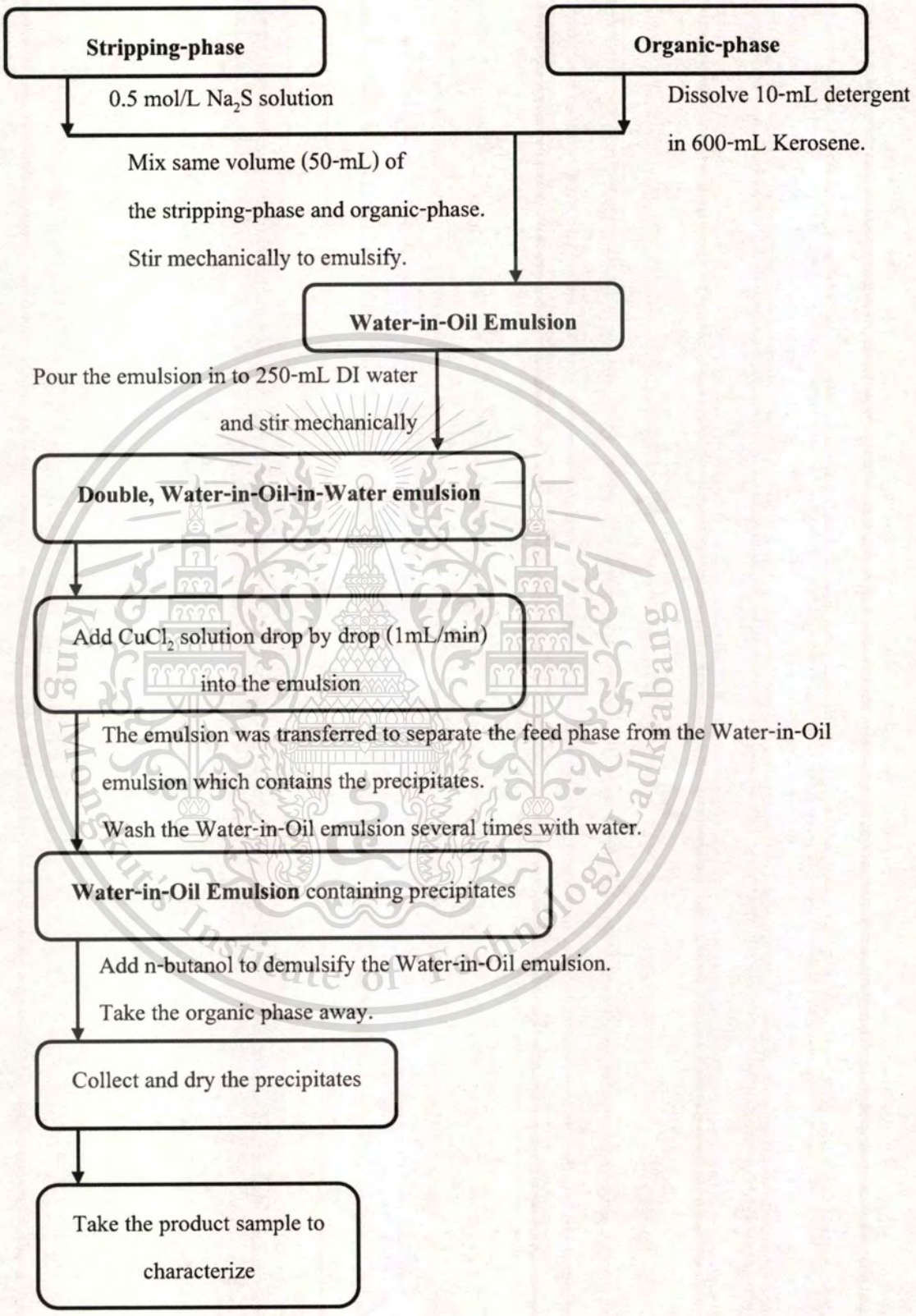

Figure 3.5: Flow diagram of Emulsion Liquid Membrane Method

Table 3.1: Synthesize condition and Sample Number

Project name	**Synthesis of Copper sulfide Nanoparticles**																	
Method	**Wet Chemical Method**												**Emulsion Liquid Membrane**					
Mole ratio $CuCl_2$:Na_2S	**1:1**						**2:1**						**1:1**			**2:1**		
Detergent	without			with			without			with								
Temperature (°C)	30	60	90	30	60	90	30	60	90	30	60	90	30	60	90	30	60	90
Sample NO.	1	2	3	5	6	7	9	10	11	13	14	15	17	18	19	21	22	23
	Ultrasonic Wash*																	
Sample NO.	1a	2a	3a	5a	6a	7a	9a	10a	11a	13a	14a	15a	17a	18a	19a	21a	22a	23a
scale up**								10s			14s							

*** Ultrasonic wash:** using ultrasonic washer to wash undesired products from sample

**** Scale up:** experimental NO.10 and NO. 14 were scaled up by repeat part 3.3.2. But amount of solutions were changed; Distilled water 150mL → 300mL, Detergent 0.1mL → 0.2mL, ($CuCl_2$) 50mL → 100mL, (Na_2S) 50mL → 100mL, and the flow rate were changed from 1mL/min to 2mL/min

3.3.4 Characterization of Products

The objective of this part of the experimental was to determine an effective method to measure the size of the particles synthesized nanoparticles Copper Sulfide and to obtain a clear image of the shape of such particles.

The following equipments were used to study the particles size during the experiment.

3.3.4.1 X-Ray Diffraction: XRD

XRD used was model D8 ADVANCE from Scientific Instruments Service Centre of KMITL. The operating conditions of the XRD instrument such as the step range and scanning range were set at 0.020° degree/sec and 20° to 70°, respectively.

3.3.4.2 X-Ray Fluorescence Spectroscopy: XRF

XRF used was model D8 SRS 3400 from Scientific Instruments Service Centre of King Mongkut's institute of Technology Ladkrabang.

3.3.4.3 Scanning Electron Microscope: SEM

The particle size and shape of products were characterized by SEM from National Metal and Materials Technology Center (MTEC).

3.3.4.4 Transmission Electron microscope: TEM

TEM used was model TECNAI 20 from Microscopic Center, Faculty of Science, Burapha University for analysis the particle size and shape.

Chapter 4

Result and Discussion

4.1 Product characterization

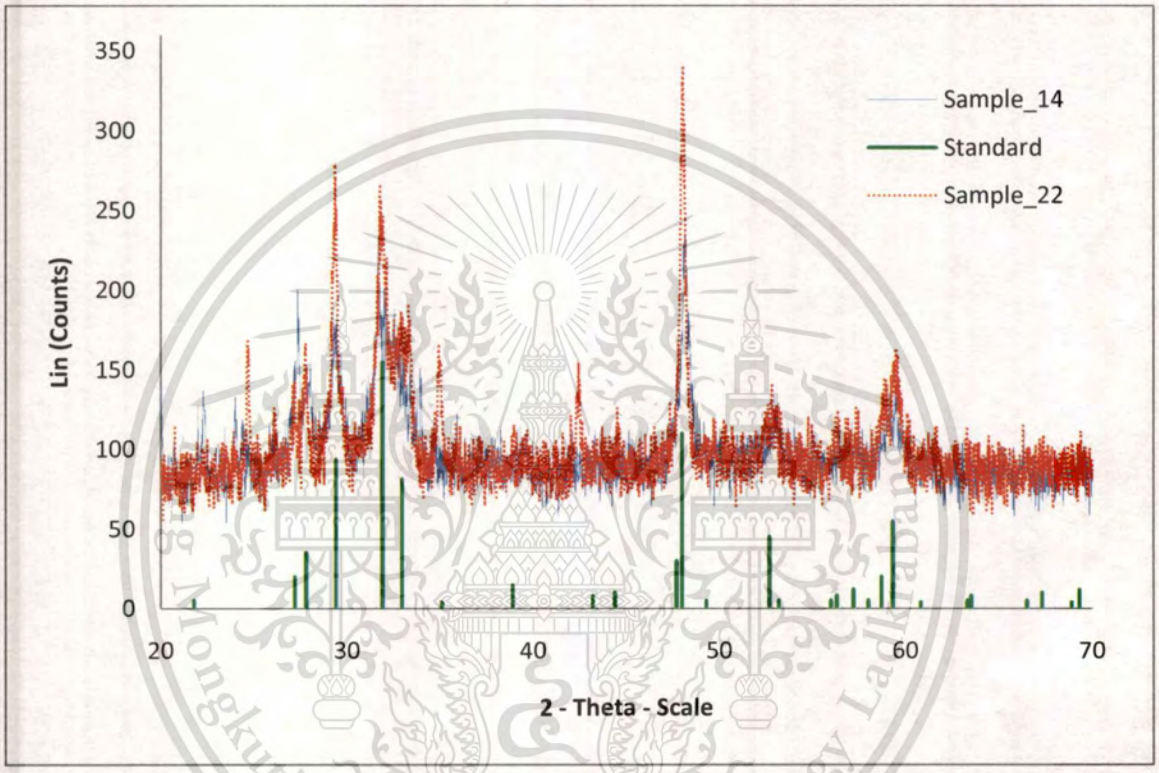

Figure 4.1: XRD Diffraction pattern of sample_14 (wet chemical method, Cu^{2+}:S^{2-}= 2:1, at 60°C, with detergent) and sample_22 (Emulsion liquid membrane, Cu^{2+}:S^{2-}= 2:1, at 60°C)

Figure 4.1 shows the diffraction pattern of sample synthesized by wet chemical method and emulsion liquid membrane method which both samples were compared with the characteristic peak of standard CuS. The diffraction patterns of samples have peaks at the same position as the standard CuS. Therefore, the samples are in good agreement with the literature data for CuS. The other samples are also in this case (XRD Diffraction pattern of all samples are shown in Appendix A.3).

Table 4.1: XRF result of sample_14 (wet chemical method, Cu^{2+}:S^{2-}= 2:1, at 60°C, with detergent) and sample_22 (Emulsion liquid membrane, Cu^{2+}:S^{2-}= 2:1, at 60°C)

	O	S	Cl	Cu	Compton	Rayleigh	Norm
Sample		76.3 KCps	6.4 KCps	1320.9 KCps			
14	39.3 %	19.9 %	1.81 %	38.7 %	1.32	1.36	100.00 %
Sample		79.5 KCps	3.9 KCps	1385.8 KCps			
22	39.7 %	20.1 %	1.06 %	38.9 %	1.34	1.36	100.00 %

Table 4.1 show weight percentages of compositions in the samples; the percentage of Oxigen is the error occurs from instrument, and Chlorine should be the remaining contaminate in form of Na_2Cl or $CuCl_2$. The percent weight of Cu:S are recalculated, the result are around 33.5:66.5 which are in good agreement with analytical data of CuS (copper (II) sulfide) or covellite in mineral name. XRF result of all samples are shown in Appendix A.2, all are in similar result as shown above.

The products synthesized from methods: wet chemical and emulsion liquid membrane, are confirmed from as CuS (copper (II) sulfide) or covellite by XRD and XRF result as shown above.

4.2 Size and Shape of particles

Table 4.2: Estimated particle size from Scherrer equation

Method	Mole ratio Of Cu^{2+}:S^{2-}	Detergent	Temperature	Sample NO.	Estimated particle size from Scherrer equation	
					At $2\theta \cong 32$	At $2\theta \cong 48$
Wet Chemical Method	1:1	without	30°C	1*	-	-
			60°C	2	7.517171	14.50758
			90°C	3	9.185356	17.40232
		with	30°C	5	6.362279	10.88069
			60°C	6	8.268888	14.50758
			90°C	7	10.33353	17.40232
	2:1	without	30°C	9	6.887301	14.51892
			60°C	10	7.513419	17.41589
			90°C	11	10.33095	21.76987
		with	30°C	13	7.513419	14.51324
			60°C	14	10.33095	17.40571
			90°C	15	11.8068	24.87985
Emulsion Liquid Membrane	1:1		30°C	17	8.264761	14.49069
			60°C	18	10.33095	21.74445
			90°C	19	11.80387	28.98137
	2:1		30°C	21	5.509841	14.4963
			60°C	22	11.8068	21.73603
			90°C	23	10.33353	14.49069

The calculation of Scherrer equation is shown in Appendix B.2.

* Sample 1: cannot calculate particle size because of a lot of noise and undesired product peak overlap with CuS peak.

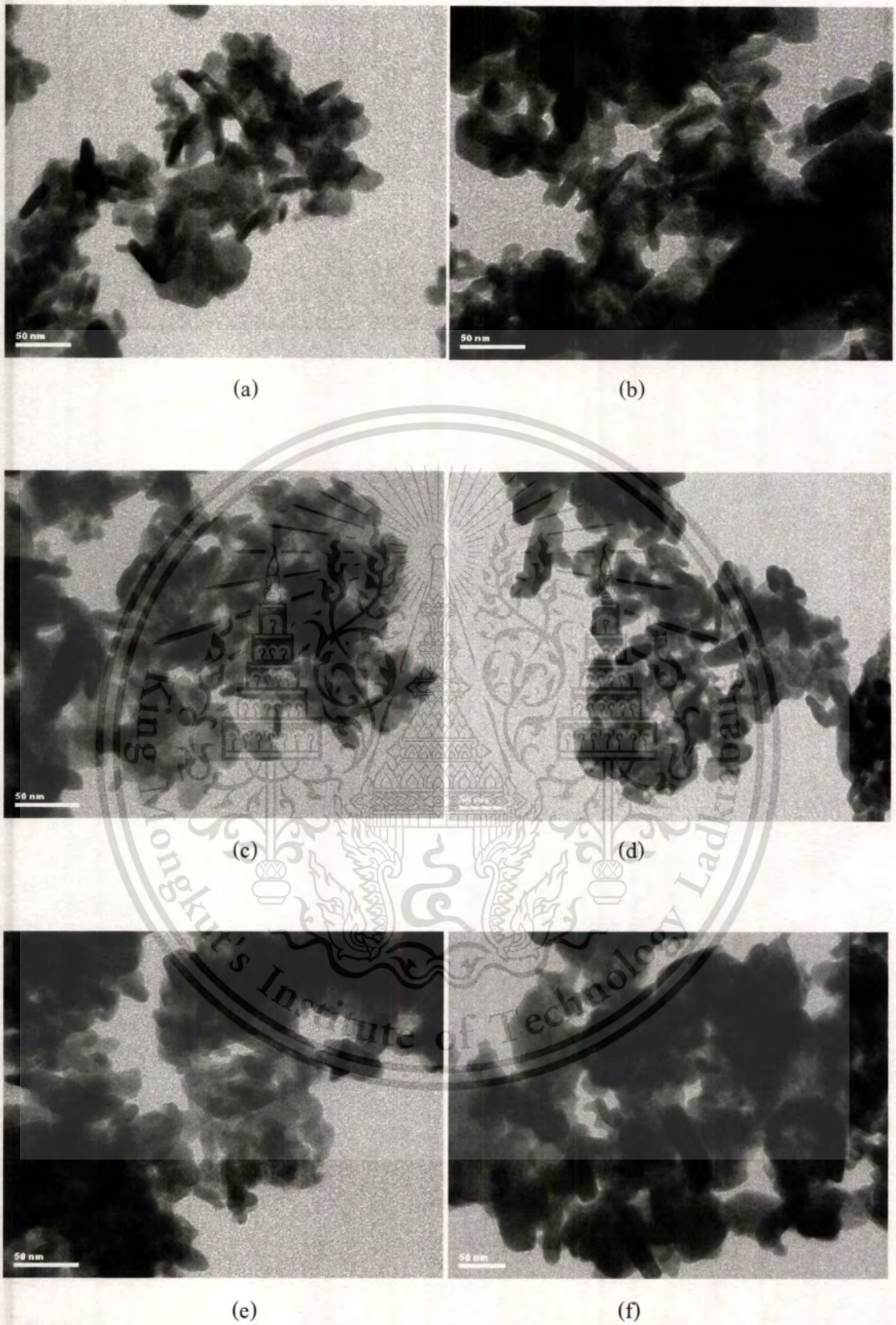

Figure 4.2: TEM image in 50 nm scale of sample 6a (a), 10a (b), 13a (c), 14a (d), 15a (e) and 22a (f)

Table 4.2 and Figure 4.2 show particle size and shape of product (CuS). From this result, it can be confirmed that synthesized of CuS by both method, wet chemical and emulsion liquid membrane, are in nanoscale. The SEM images also show that the shape of particles is rod-shaped. The mean width of rods particles obtained from TEM images are close to particle size calculated by Scherrer equation.

The effect of synthesize method, temperature, mole ratio and detergent (in wet chemical method) are discussed following

4.2.1 Effect of synthesize method

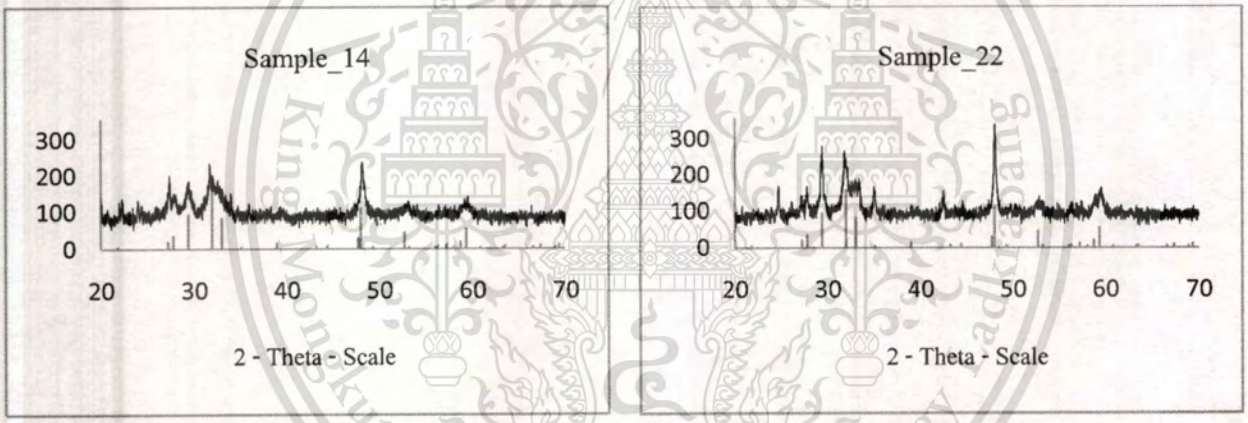

Figure 4.3: Comparisons of XRD spectra of sample14 (wet chemical method, Cu^{2+}:S^{2-} = 2:1, at 60°C, with detergent) and sample_22 (Emulsion liquid membrane, Cu^{2+}:S^{2-} = 2:1, at 60°C)

The comparisons of XRD spectra shows that synthesize of CuS by emulsion liquid membrane obtain higher crystallinity particles than synthesize by wet chemical method. The crystallinity of particles is illustrated in high intensity of characteristic pattern of sample. The high intensity of characteristic pattern also leads to narrow FWHM, which is used in calculation of particle size by Scherrer equation, this effect cause the particle size to be larger. The results are in agreement with the particle size illustrated by TEM image (all images are shown in Appendix A.5)

4.2.2 Effect of temperature

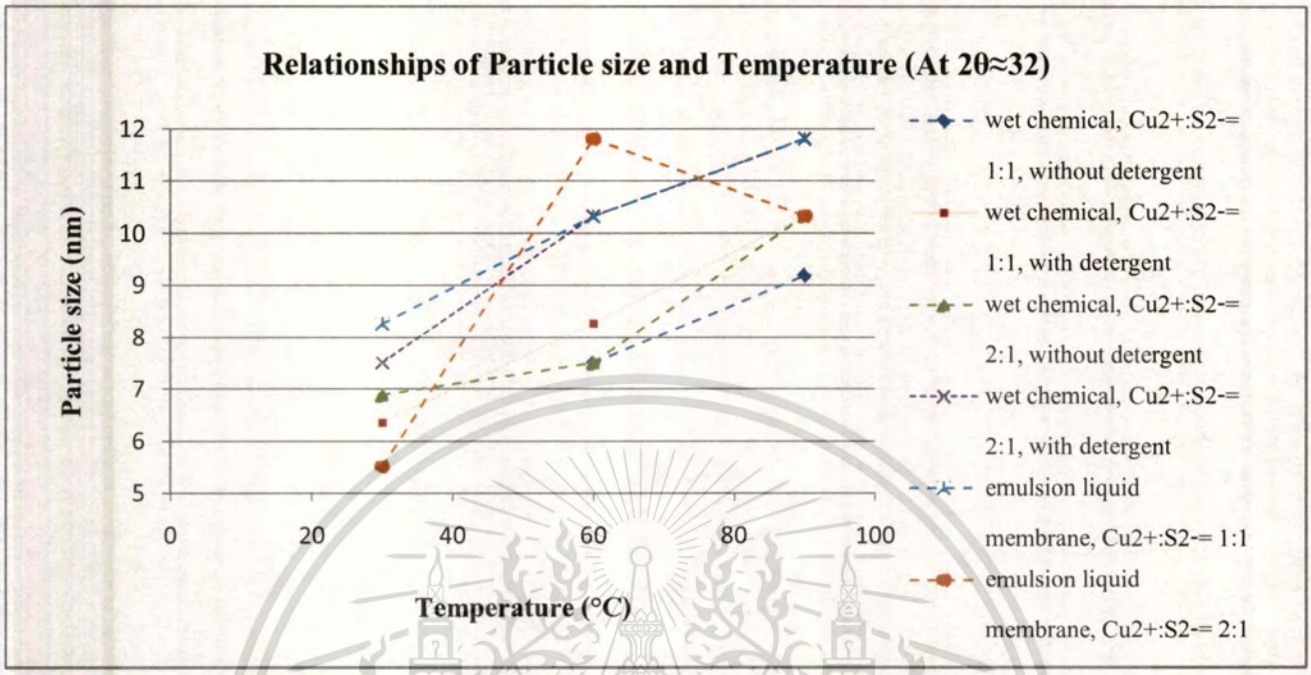

Figure 4.4: Chart of Relationships of Particle size (calculated from Scherrer equation at $2\theta \cong 32$) and Temperature

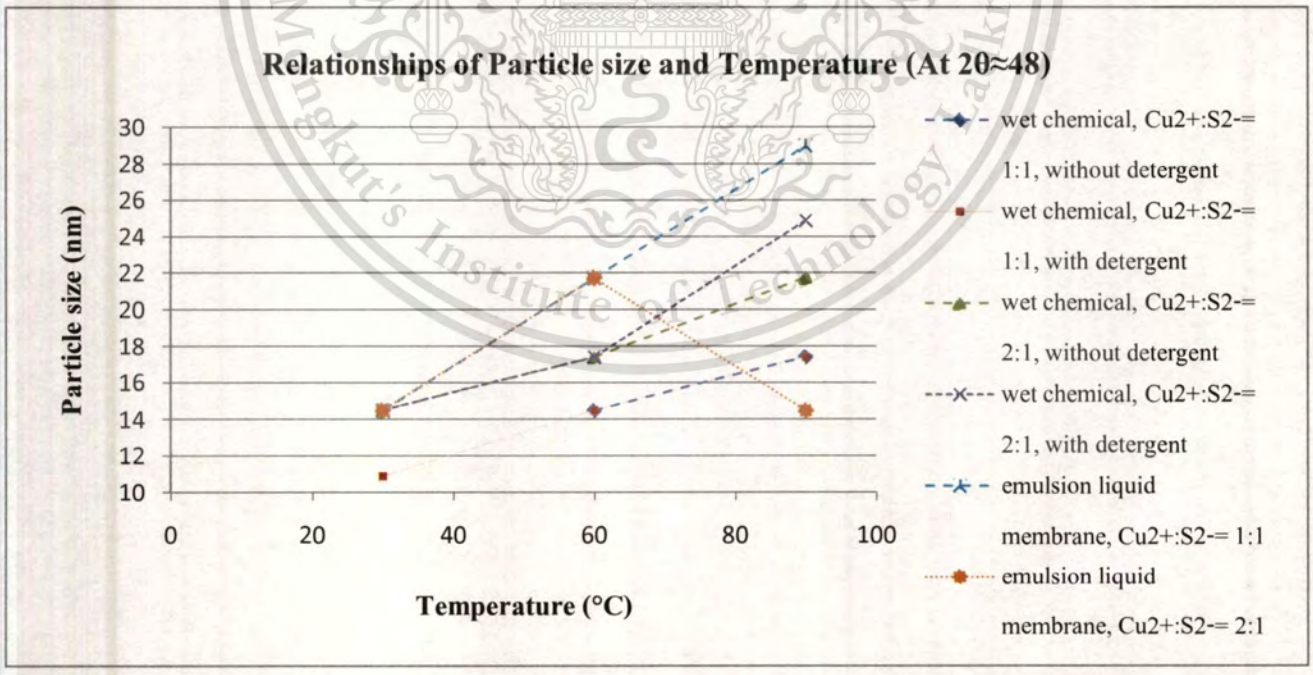

Figure 4.5: Chart of Relationships of Particle size (calculated from Scherrer equation at $2\theta \cong 48$) and Temperature

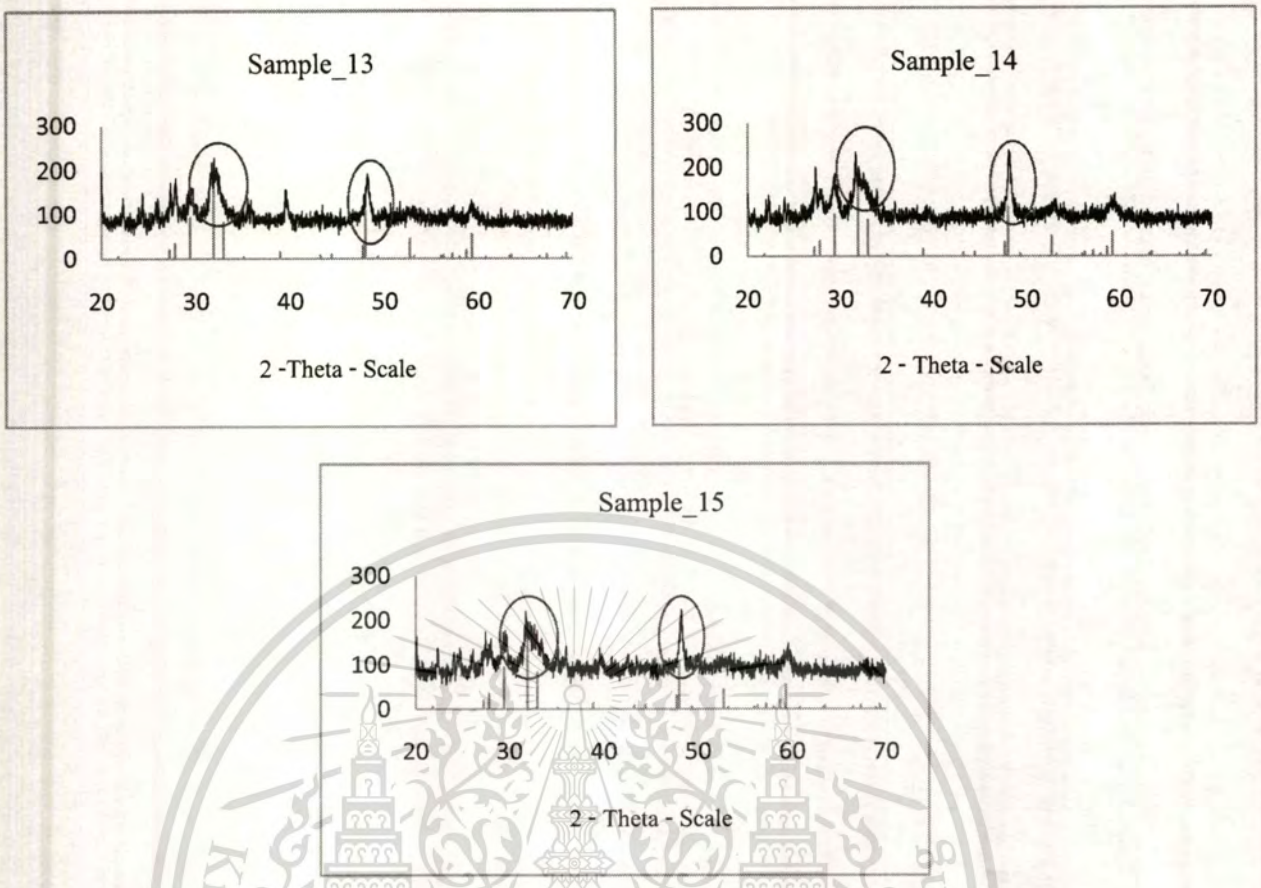

Figure 4.6: Comparisons of XRD spectra of sample synthesized by wet chemical method, Cu^{2+}:S^{2-} = 2:1, with detergent; sample 13 (at 30°C), sample 14 (at 60°C) and sample 15 (at 90°C)

In Figure 4.4 and 4.5, the particle size calculated from Scherrer equation are increasing when synthesizes at higher temperature, except the result from emulsion liquid membrane with Cu^{2+}:S^{2-} = 2:1. The result from XRD spectra (see Figure 4.6) illustrated that, the higher the temperature, the characteristic peaks are higher in intensity and tend to be narrower than lower temperature, which resulted in larger particle size as shown in Table 4.2. The TEM images (Figure 4.2 and all images are in Appendix A.5) are also in the same way, at higher temperature (sample 15a) the particles width are larger, but a little shorter in length. At low temperature (sample 13a) the width of rods is less than of sample 14a and 15a.

4.2.3 Effect of mole ratio

Figure 4.4 and 4.5 show that in wet chemical method, particles size of mole ratio Cu^{2+}:S^{2-}= 2:1 are larger than particles synthesized at mole ratio Cu^{2+}:S^{2-}= 1:1. For emulsion liquid membrane, particle sizes calculated from Scherrer equation that there are no trends of effect of mole ratio.

(6a) (14a)

Figure 4.7: Comparisons of TEM images of sample synthesized by wet chemical method, at 60°C, with detergent; sample 6a (at Cu^{2+}:S^{2-} = 1:1) and sample 14a (Cu^{2+}:S^{2-}= 2:1)

The results of wet chemical method are also confirmed by Figure 4.7, the widths of rods of sample 14a are larger than of sample 6a.

4.2.4 Effect of detergent (in wet chemical method)

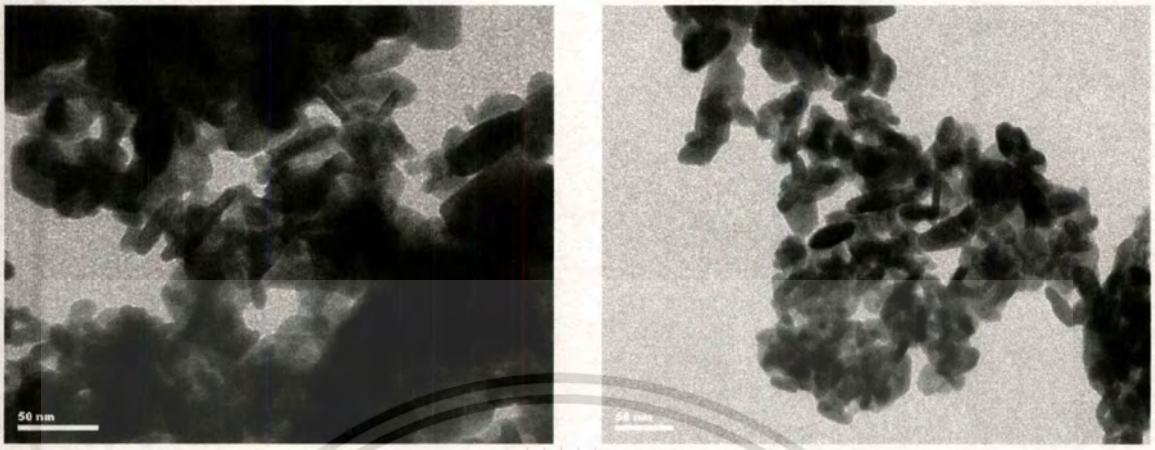

(10a) (14a)

Figure 4.8: Comparisons of TEM images of sample synthesized by wet chemical method, at 60°C, Cu^{2+}:S^{2-} = 2:1; sample 6a (without detergent) and sample 14a (with detergent)

There are no significantly effects of detergent on particles size and shape. But from TEM images, the particles synthesized without detergent are likely to be occurred of agglomeration.

4.3 Percent yield of product

Table 4.3: Percent yield of product

Method	Mole ratio Of Cu^{2+}:S^{2-}	Detergent	Temperature	Sample NO.	Percent yield
Wet Chemical Method	1:1	without	30°C	1	87.86611
			60°C	2	71.64435
			90°C	3	98.05021
		with	30°C	5	73.11715
			60°C	6	70.61506
			90°C	7	99.58577
	2:1	without	30°C	9	115.4686
			60°C	10	102.1423
			90°C	11	114.749
		with	30°C	13	115.1715
			60°C	14	105.3096
			90°C	15	111.7029
Emulsion Liquid Membrane	1:1		30°C	17	92.38075
			60°C	18	91.46862
			90°C	19	91.66109
	2:1		30°C	21	89.63598
			60°C	22	85.07531
			90°C	23	85.22176
Scale up	2:1	without	60°C	10s	81.94142
	2:1	with	60°C	14s	80.45188

Table 4.3 shows percent yield of copper sulfide products at each condition. There are no effects of temperature, mole ratio of Cu^{2+}:S^{2-}, and synthesis method. The errors may occur from;

- Contaminant of reactant such as Na_2S, $CuCl_2$ and detergent
- Loss of sample during filtration

The experimental data are shown in Appendix A.1 and calculation method are shown in Appendix B.1

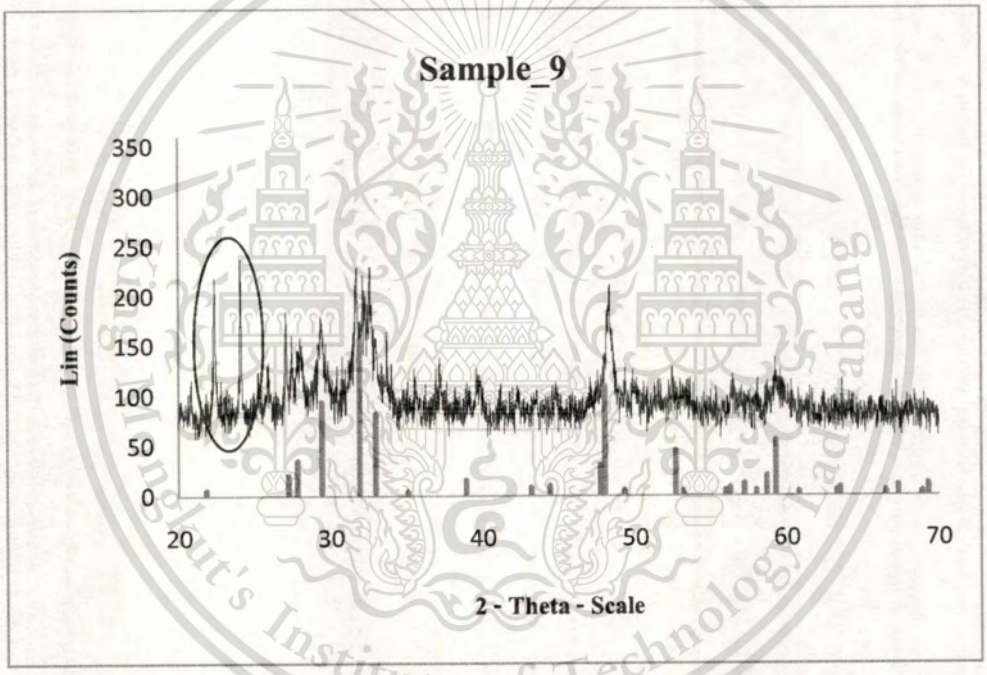

Figure 4.9: XRD spectra of sample 9 show contaminant in sample

Chapter 5

Conclusion and Recommendation

5.1 Conclusion

Wet chemical method and emulsion liquid membrane were use to synthesize CuS nanoparticles in this specials project. The particles sizes of product are in nano-range (from 5 nm – 29 nm) and in rod-shaped. The temperature affects on size and shape of particle, the higher temperatures, the larger width of rod and particle shape are likely to be rounder. Synthesizing by emulsion liquid membrane, the particles have higher crystallinity than synthesizing by wet chemical method, also sizes of particles are larger. The suitable method for photovoltaic materials manufacturing should be emulsion liquid membrane because of the higher crystallinity of Copper Sulfide nanoparticle produced.

5.2 Recommendation

For further study, these two methods, wet chemical method and emulsion liquid membrane, should be done in larger scale and in more various conditions such as at higher temperature, pressure or use other starting materials. Furthermore, a detailed study of temperature would be beneficial in predicting particle size and shape. The study of kinematic would also useful for size and shape controlling. The problem of losing of sample during should be solved by using sintered crucible instead of Buchner funnel.

Reference

[1] Santosh K.; Anand R.M.; Sharad G.,J. Phys. Chem., 1996, 6

[2] M. B. Muradov; A. Sh. Abdinov; R. H. Hajimamedov; G. M. Eyivazova, Surf. Engineering and A. Electrochemistry, 2009,

[3] Xinyu S.; Sixiu S.; Weimin Z.; Zhilei Y., J. Colloid and Interface Sci., 2004, 6

[4] Lisiecki; F.Billouder; M.P.Pileni, J. Mol. Liquids, 1997, 11

[5] Copper monosulfide. Wikipedia, the free encyclopedia. Available: http://en.wikipedia.org/wiki/copper_monosulfide

[6] Copper sulfde. Wikipedia, the free encyclopedia. Available: http://en.wikipedia.org/wiki/ copper_sulfide

[7] M.T. Sebastian. Dielectric Materials for Wireless communication, 1st ed. Great Britain: Elsevier publication, 2008, ch.4, p 84.

[8] Nanoparticle. Wikipedia, the free encyclopedia. Available: http://en.wikipedia.org/wiki/Nanoparticle

[9] Dry media reaction. Wikipedia, the free encyclopedia. Available: http://en.wikipedia.org/wiki/Solid-state_reaction

[10] Xiaohong Kang and Bin Wang. (2007, Sep.). Synthesis and tribological property study of oleic acid-modified copper sulfide nanoparticles. Elsivier [online]. Available: http://www.elsivier.com/locate/wear

[11] P.S. Khiew and S. Radiman. (2004, May.). Syntesis and characterization of copper sulfide Nanoparticles in hexagonal phase lyotropic liquid crystal. Elsivier [online]. Available: http://www.elsivier.com/locate/jcrysgro

[12] Ujjal K Gautam and Bratindranath Mukherjee. (2005, Nov.). A simple synthesis and Characterization of CuS nanocrystals. Bull. Mater. Sci., vol. 29, No. 1, February 2006, pp.1-5

[13] Jia Xu and Xuejun Cui. (2008, Jan.). Preparation of CuS nanoperticles embedded in Poly(vinyl alcohol) nanofibre via electrospinning. Bull. Mater. Sci., vol. 31, No. 2, April 2008, pp. 189-192

[14] Xu-Sheng Du and Mosong. (2008, Mar.). Shape-controlled Synthesis and Assembly of Copper Sulfide nanoparticles. Crystal Growth & Design, vol. 8, No. 6, 2008, pp. 2032-2035

[15] Kaibin Tang and Di Chen. (2003, Nov.). Shaped-controlled synthesis of copper sulfide nanocrystals via a soft solution route. Elsivier [online]. Available: http://www.elsivier.com/locate/jcrysgro

[16] Santosh K. and Anand R. (1995, Dec.). Synthesis and characterization of Copper Sulfide nanopartickes in triton-X 100 Water-in-oil Microemulsions. J. Phys. Chem. Vol. 100, No. 14, 1996, pp. 5868-5873

[17] A.E. Raevskaya and A.L. Stroyuk. (2003, Oct.). Synthesis and Photophysical properties of CuS nanoparticles stabilized by sodium polyphosphate. Theoretical and Experimental Chemistry. Vol. 39, No. 5, 2003, pp. 303-308

[18] Mousa Al-Tarazi and Mohammed O.J. (2005, Jan.). Precipitation of CuS and ZnS in a Bubble Column Reactor. AIChE Journal. Vol. 51, No. 1, January 2005, pp. 235-246

[19] Chunyan Wu and Shu-Hong Yu. (2006, June). Large scale synthesis of uniform CuS nanotubes in ethylene glycol by a sacrificial templating method under mild conditions. J. Mater. Chem., 2006, 16, pp.3326-3331

[20] Poulomi Roy and Suneel Kumar Srivastava. (2006, July). Low-temperature synthesis of CuS nanorods by simple wet chemical method. Elsivier [online]. Available: http://www.elsivier.com/locate/matlet

[21] Keitaro Tezuka and William C. Sheets. (2006, Oct.). Synthesis of covellite (CuS) from the Elements. Elsivier [online]. Available: http://www.elsivier.com/locate/ssscie

[22] Lihua Wang and Chao Xu. (2008, June). Synthesis of hierarchical CuS flower-like submicorspheres via an ionic liquid-assisted route. Bull. Mater. Sci., vol. 31, No. 7, December 2008, pp. 931-935

[23] Ding Tong-Yang and Guo Guo-Cong. (2008, March). Mild-temperature Synthesis of Covallite Copper Sulfide Hexagonal Nanoplatelets via the Hydrothermal Route. Chinese J. Struct. Chem. Vol. 28, No. 1, 2009, pp. 19-24

[24] Limei Xu and Xio Chen. (2009, July). Facile preparation of copper sulfide nanoparticles From perovskite templates containing bromide anions. Elsivier [online]. Available: http://www.elsivier.com/locate/colsurfa

[25] Ritika Gupta, "Snthesis of precipitated calcium carbonate nanoparticles using midified emulsion liquid membranes," Georgia Institute of Technology, May 2004

[26] Covellite Mineral Data. Dakota Matrix Minerals. Available: http://webmineral.com/data/Covellite.shtml

[27] Covellite: covellite mineral information and data. Mindat.org. Available: http://www.mindat.org/min-1144.html

[28] Copper(II) sulfide. NIST and CSTL. Available: http://webbook.nist.gov/cgi/cbook.cgi?ID=C1317404&Units=CAL&Mask=1000

[29] C.M. Simonescu; I. Patron; J. optoelectronic and A. materials, p 597-600

[30] Santheep K. Mathew; N.P. Rajesh; Masaya Ichimura; Material Letter 62, p.591-593

[31] R. Bernal; F.J. Espinoza; Superficies y Vacio 9, p.219-221

[32] Krishna Veer Singh1; Alfredo A. Martinez-Morales; and Mihrimah Ozkan; Mater. Res. Soc. Symp. Proc. Vol. 1018, 7

[33] X-ray Crystallography. Wikipedia, the free encyclopedia. Available: http://en.wikipedia.org/wiki/X-ray_crystallography

[34] Shape Factor (X-ray diffraction). Wikipedia, the free encyclopedia. Available: http://en.wikipedia.org/wiki/Shape_factor_(X-ray_diffraction)

[35] Sathish Sukumaran's Derivation of Scherrer Equation. Available: http://www.eng.uc.edu/~gbeaucag/Classes/XRD/SathishScherrerhtml/SathishScherrerEqn.html

[36] X-ray fluorescence. Wikipedia, the free encyclopedia. Available: http://en.wikipedia.org/wiki/X-ray_fluorescence

[37] Scanning Electron Microscope . Wikipedia, the free encyclopedia. Available: http://en.wikipedia.org/wiki/Scanning_electron_microscope

[38] Transmission electron microscopy. Wikipedia, the free encyclopedia. Available: http://en.wikipedia.org/wiki/Transmission_electron_microscopy

APPENDICES

Appendix A

Experimental Data

A.1 Data Recorded

A.1.1 Wet Chemical Method

Table A.1: The experimental data of wet chemical method

Sample NO.	Experimental date	weight(g)		
		filter paper + watch glass	filter paper + watch glass + sample	sample
1	Nov. 23, 2009	57.1	59.2	2.1
2	Nov. 23, 2009	35.1537	36.866	1.7123
3	Nov. 23, 2009	31.2835	33.6269	2.3434
5	Dec. 8, 2009	0.4545	2.202	1.7475
6	Dec. 8, 2009	0.4545	2.1422	1.6877
7	Dec. 9, 2009	32.1513	34.5314	2.3801
9	Dec. 8, 2009	29.1543	31.914	2.7597
10	Dec. 8, 2009	32.3458	34.787	2.4412
11	Dec. 8, 2009	33.5177	36.2602	2.7425
13	Dec. 9, 2009	60.6484	63.401	2.7526
14	Dec. 9, 2009	34.6993	37.2162	2.5169
15	Dec. 9, 2009	33.5116	36.1813	2.6697

A.1.2 Emulsion Liquid Membrane

Table A.2: The experimental data of emulsion liquid membrane

Sample NO.	Experimental date	weight(g)		
		filter paper + watch glass	filter paper + watch glass + sample	sample
17	Jan. 19, 2010	33.5041	35.712	2.2079
18	Jan. 19, 2010	34.6989	36.885	2.1861
19	Jan. 19, 2010	30.8423	33.033	2.1907
21	Jan. 19, 2010	61.3247	63.467	2.1423
22	Jan. 19, 2010	31.5167	33.55	2.0333
23	Jan. 19, 2010	32.7882	34.825	2.0368

A.1.3 Scale up

Table A.3: The experimental data of scale up (wet chemical method)

Sample NO.	Experimental date	weight(g)		
		filter paper + watch glass	filter paper + watch glass + sample	sample
10s	Feb. 2, 2010	39.6094	43.5262	3.9168
14s	Feb. 2, 2010	34.8626	38.7082	3.8456

A.2 XRF Data

Table A.4: XRF data of sample_1

Printed by Eval on 26-Jan-2010 12:36:30

Sample: XF53_0012_01_Sample_1

Sample measured on 15-Jan-2010 12:47:35

O	S	Cl	Cu	Compton	Rayleigh	Norm
	48.2 KCps	5.1 KCps	127.9 KCps			
35.0 %	15.6 %	1.74 %	47.4 %	1.10	1.34	100.00 %

Table A.5: XRF data of sample_2

Printed by Eval on 26-Jan-2010 12:36:36

Sample: XF53_0012_02_Sample_2

Sample measured on 15-Jan-2010 13:05:20

O	S	Cl	Cu	Compton	Rayleigh	Norm
	76.2 KCps	7.9 KCps	1319.2 KCps			
39.2 %	20.0 %	2.24 %	38.3 %	1.33	1.36	100.00 %

Table A.6: XRF data of sample_3

Printed by Eval on 26-Jan-2010 12:36:42

Sample: XF53_0012_03_Sample_3

Sample measured on 15-Jan-2010 13:22:53

O	S	Cl	Cu	Compton	Rayleigh	Norm
	79.1 KCps	3.6 KCps	1349.9 KCps			
40.0 %	20.4 %	1.00 %	38.4 %	1.38	1.48	100.00 %

Table A.7: XRF data of sample_5

Printed by Eval on 26-Jan-2010 12:36:47

Sample: XF53_0012_05_Sample_5

Sample measured on 15-Jan-2010 13:40:11

O	S	Cl	Cu	Compton	Rayleigh	Norm
	62.7 KCps	8.4 KCps	1300.7 KCps			
36.9 %	17.9 %	2.59 %	42.5 %	1.23	1.29	100.00 %

Table A.8: XRF data of sample_6

Printed by Eval on 26-Jan-2010 12:36:50

Sample: XF53_0012_06_Sample_6

Sample measured on 15-Jan-2010 13:57:27

O	S	Cl	Cu	Compton	Rayleigh	Norm
	72.9 KCps	9.8 KCps	1259.6 KCps			
38.6 %	19.5 %	2.83 %	37.9 %	1.27	1.43	100.00 %

Table A.9: XRF data of sample_7

Printed by Eval on 26-Jan-2010 12:36:54

Sample: XF53_0012_07_Sample_7

Sample measured on 15-Jan-2010 14:14:45

O	S	Cl	Cu	Compton	Rayleigh	Norm
	78.1 KCps	4.0 KCps	1324.0 KCps			
40.1 %	20.5 %	1.14 %	38.2 %	1.37	1.41	100.00 %

Table A.10: XRF data of sample_9

Printed by Eval on 26-Jan-2010 12:36:58

Sample: XF53_0012_09_Sample_9

Sample measured on 15-Jan-2010 14:32:19

O	S	Cl	Cu	Compton	Rayleigh	Norm
	64.6 KCps	8.2 KCps	1227.3 KCps			
37.8 %	18.8 %	2.58 %	40.8%	1.22	1.29	100.00 %

Table A.11: XRF data of sample_10

Printed by Eval on 26-Jan-2010 12:37:10

Sample: XF53_0012_10_Sample_10

Sample measured on 15-Jan-2010 14:49:35

O	S	Cl	Cu	Compton	Rayleigh	Norm
	75.6 KCps	8.8 KCps	1283.3 KCps			
39.1 %	20.0 %	2.52 %	38.3 %	1.30	1.34	100.00 %

Table A.12: XRF data of sample_11

Printed by Eval on 26-Jan-2010 12:37:48

Sample: XF53_0012_11_Sample_11

Sample measured on 19-Jan-2010 14:27:17

O	S	Cl	Cu	Compton	Rayleigh	Norm
	65.5 KCps	8.2 KCps	1343.8 KCps			
37.1 %	18.1 %	2.43 %	42.3 %	1.25	1.30	100.00 %

Table A.13: XRF data of sample_13

Printed by Eval on 26-Jan-2010 12:38:37

Sample: XF53_0012_13_Sample_13

Sample measured on 19-Jan-2010 14:45:17

O	S	Cl	Cu	Compton	Rayleigh	Norm
	66.6 KCps	12.4 KCps	1280.5 KCps			
37.0 %	18.3 %	3.66 %	39.9 %	1.30	1.32	100.00 %

Table A.14: XRF data of sample_14

Printed by Eval on 26-Jan-2010 12:40:04

Sample: XF53_0012_14_Sample_14

Sample measured on 19-Jan-2010 15:02:33

O	S	Cl	Cu	Compton	Rayleigh	Norm
	76.3 KCps	6.4 KCps	1320.9 KCps			
39.3 %	19.9 %	1.81 %	38.7 %	1.32	1.36	100.00 %

Table A.15: XRF data of sample_15

Printed by Eval on 26-Jan-2010 12:40:07

Sample: XF53_0012_15_Sample_15

Sample measured on 19-Jan-2010 15:19:49

O	S	Cl	Cu	Compton	Rayleigh	Norm
	67.8 KCps	7.1 KCps	1319.7 KCps			
37.9 %	18.6 %	2.11 %	41.1 %	1.27	1.32	100.00 %

Table A.16: XRF data of sample_17

Printed by Eval on 19-Feb-2010 11:24:44

Sample: XF53_0021_01_Sample_17

Sample measured on 16-Feb-2010 14:05:27

O	S	Cl	Cu	Compton	Rayleigh	Norm
	69.5 KCps	6.3 KCps	1439.1 KCps			
37.4 %	17.9 %	1.75 %	41.5 %	1.33	1.32	100.00 %

Table A.17: XRF data of sample_18

Printed by Eval on 19-Feb-2010 11:24:54

Sample: XF53_0021_01_Sample_18

Sample measured on 16-Feb-2010 14:23:45

O	S	Cl	Cu	Compton	Rayleigh	Norm
	73.3 KCps	5.5 KCps	1390.8 KCps			
38.5 %	18.9 %	1.51 %	39.8 %	1.34	1.46	100.00 %

Table A.18: XRF data of sample_19

Printed by Eval on 19-Feb-2010 11:25:00

Sample: XF53_0021_03_Sample_19

Sample measured on 16-Feb-2010 14:41:00

O	S	Cl	Cu	Compton	Rayleigh	Norm
	79.0 KCps	3.4 KCps	1402.1 KCps			
39.6 %	19.9 %	0.937 %	39.3 %	1.35	1.50	100.00 %

Table A.19: XRF data of sample_21

Printed by Eval on 19-Feb-2010 11:25:07

Sample: XF53_0021_04_Sample_21

Sample measured on 16-Feb-2010 14:58:16

O	S	Cl	Cu	Compton	Rayleigh	Norm
	72.9 KCps	4.7 KCps	1398.0 KCps			
38.7 %	19.2 %	1.33%	40.7 %	1.34	1.38	100.00 %

Table A.20: XRF data of sample_22

Printed by Eval on 19-Feb-2010 11:25:14

Sample: XF53_0021_05_Sample_22

Sample measured on 16-Feb-2010 15:15:33

O	S	Cl	Cu	Compton	Rayleigh	Norm
	79.5 KCps	3.9 KCps	1385.8 KCps			
39.7 %	20.1 %	1.06 %	38.9 %	1.34	1.36	100.00 %

Table A.21: XRF data of sample_23

Printed by Eval on 19-Feb-2010 11:25:21

Sample: XF53_0021_06_Sample_23

Sample measured on 16-Feb-2010 15:32:51

O	S	Cl	Cu	Compton	Rayleigh	Norm
	79.2 KCps	4.4 KCps	1362.0 KCps			
39.8 %	20.2%	1.21 %	38.6 %	1.35	1.37	100.00 %

A.3 XRD Data

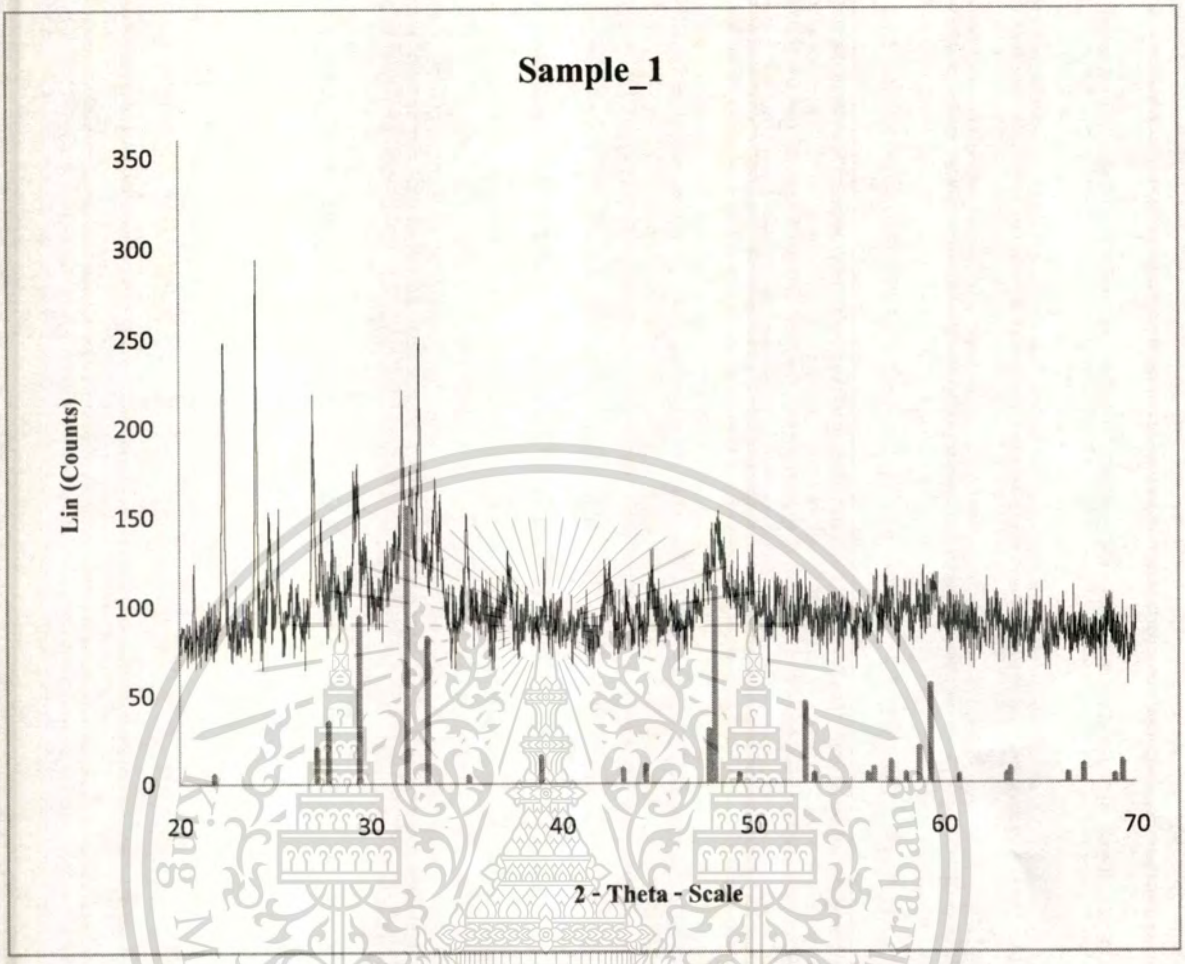

Figure A.1: X-ray Diffraction pattern of sample_1

Sample_1 – File:1XD53_0032_01_sample_1.RAW – Type: 2Th/Th locked – Start: 20.000° - End: 70.000° -Step: 0.020° - Step time: 1.s – Temp.: 25°C (Room) – Time Started: 0 s – 2 – Theta: 20.000° - Theta: 10.000° - Operations: Import

79 - 2321 (C) - Copper Sulfide – CuS – Y: 50.00 % - d x by: 1. – WL: 1.5406 – Hexagonal-a 3.78813 – b 3.78813 – c 16.33307 – alpha 90.000 – beta 90.000 – gamma 120.000 – Primitive – P63/mmc (194) – 6 – 202.978 – I/Ic P

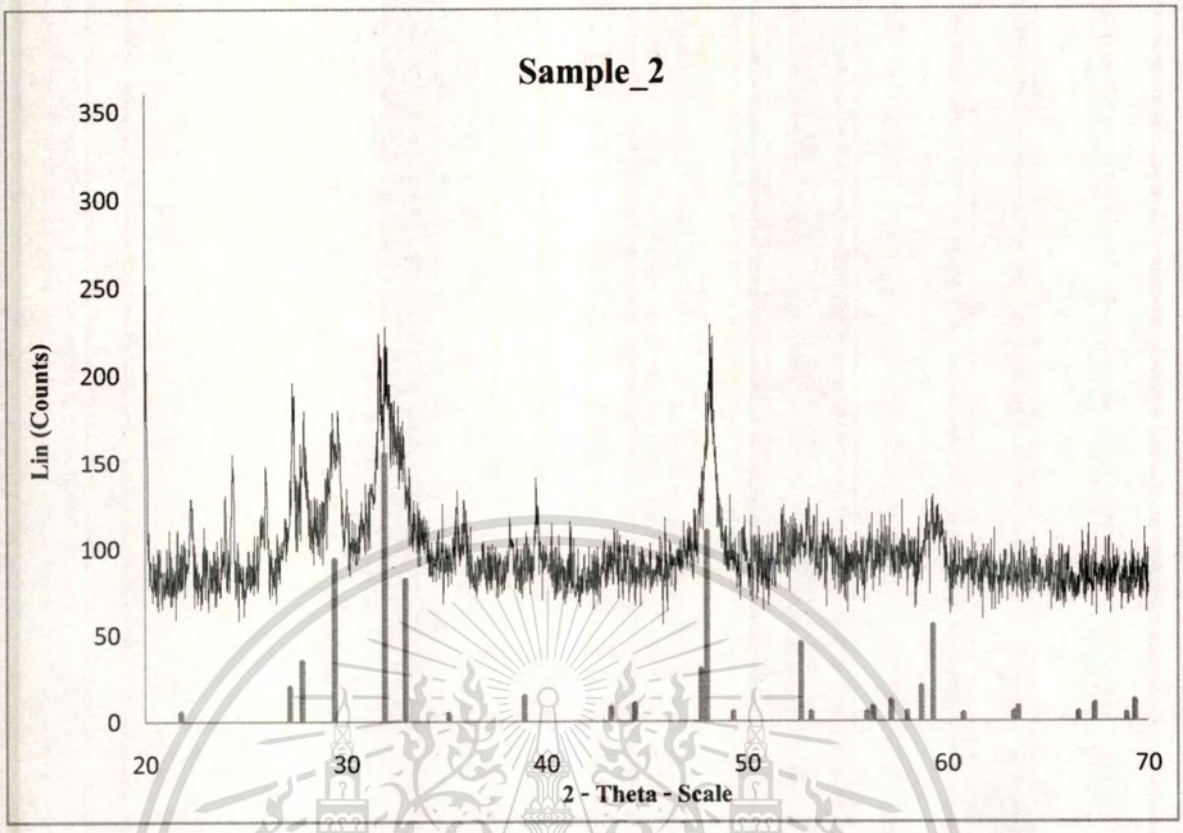

Figure A.2: X-ray Diffraction pattern of sample_2

Sample_2 – File:1XD53_0032_02_sample_2.RAW – Type: 2Th/Th locked – Start: 20.000° - End: 70.000° -Step: 0.020° - Step time: 1.s – Temp.: 25°C (Room) – Time Started: 0 s – 2 – Theta: 20.000° - Theta: 10.000° - Operations: Import

79 - 2321 (C) - Copper Sulfide – CuS – Y: 50.00 % - d x by: 1. – WL: 1.5406 – Hexagonal-a 3.78813 – b 3.78813 – c 16.33307 – alpha 90.000 – beta 90.000 – gamma 120.000 – Primitive – P63/mmc (194) – 6 – 202.978 – I/Ic P

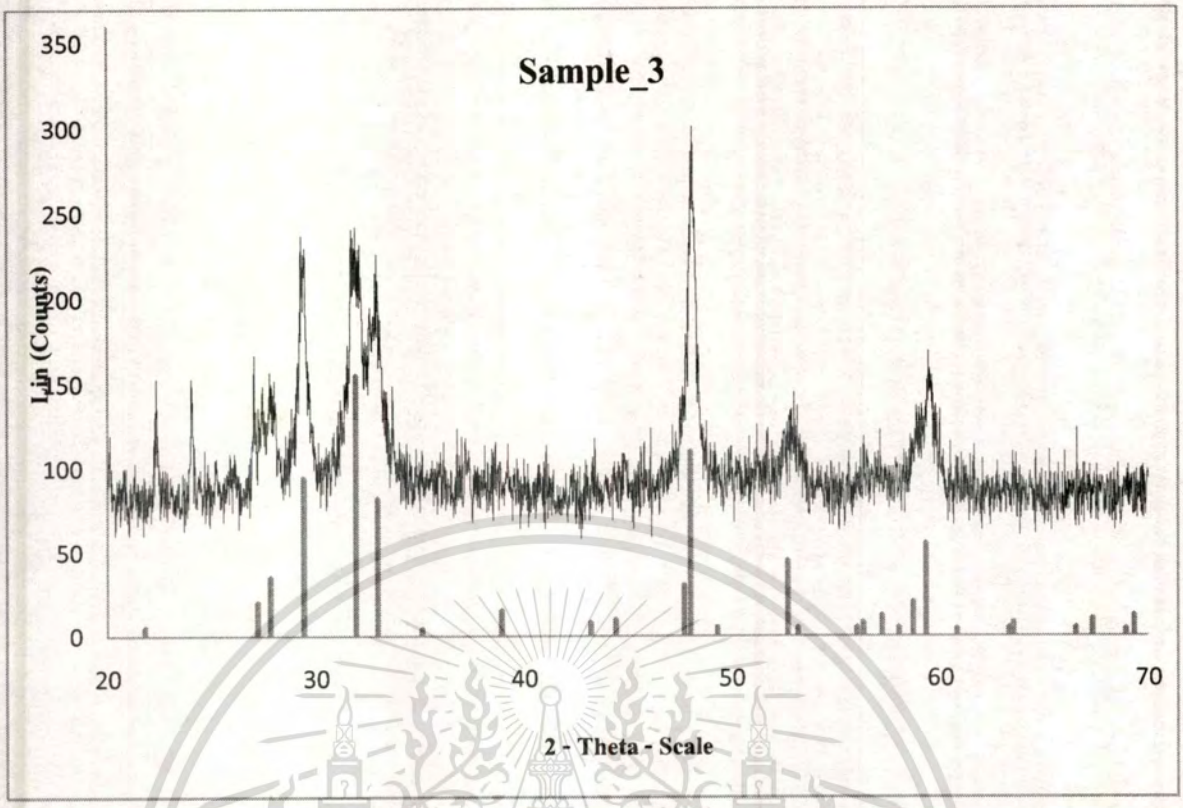

Figure A.3: X-ray Diffraction pattern of sample_3

Sample_3 – File:1XD53_0032_03_sample_3.RAW – Type: 2Th/Th locked – Start: 20.000° - End: 70.000° -Step: 0.020° - Step time: 1.s – Temp.: 25°C (Room) – Time Started: 0 s – 2 – Theta: 20.000° - Theta: 10.000° - Operations: Import

79 - 2321 (C) - Copper Sulfide – CuS – Y: 50.00 % - d x by: 1. – WL: 1.5406 – Hexagonal-a 3.78813 – b 3.78813 – c 16.33307 – alpha 90.000 – beta 90.000 – gamma 120.000 – Primitive – P63/mmc (194) – 6 – 202.978 – I/Ic P

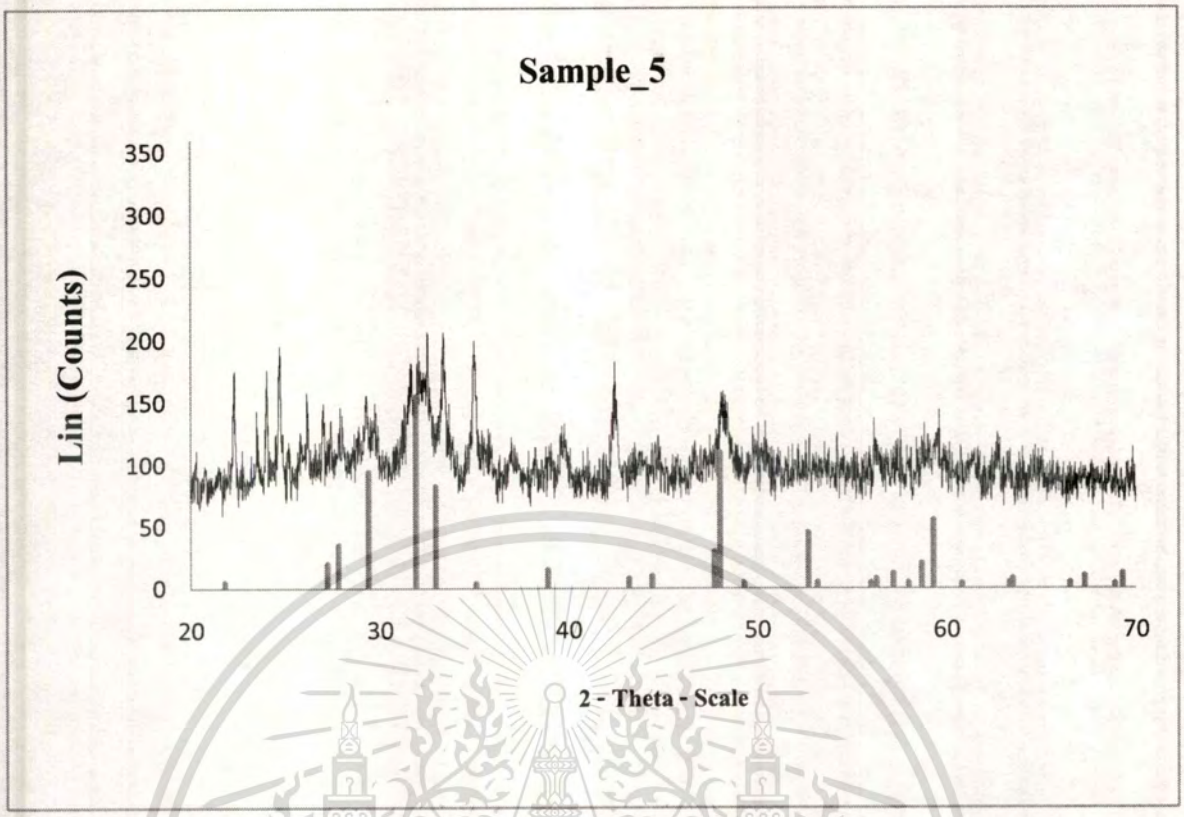

Figure A.4: X-ray Diffraction pattern of sample_5

Sample_5 – File:1XD53_0032_04_sample_5.RAW – Type: 2Th/Th locked – Start: 20.000° - End: 70.000°-Step: 0.020° - Step time: 1.s – Temp.: 25°C (Room) – Time Started: 0 s – 2 – Theta: 20.000° - Theta: 10.000° - Operations: Import

79 - 2321 (C) - Copper Sulfide – CuS – Y: 50.00 % - d x by: 1. – WL: 1.5406 – Hexagonal-a 3.78813 – b 3.78813 – c 16.33307 – alpha 90.000 – beta 90.000 – gamma 120.000 – Primitive – P63/mmc (194) – 6 – 202.978 – I/Ic P

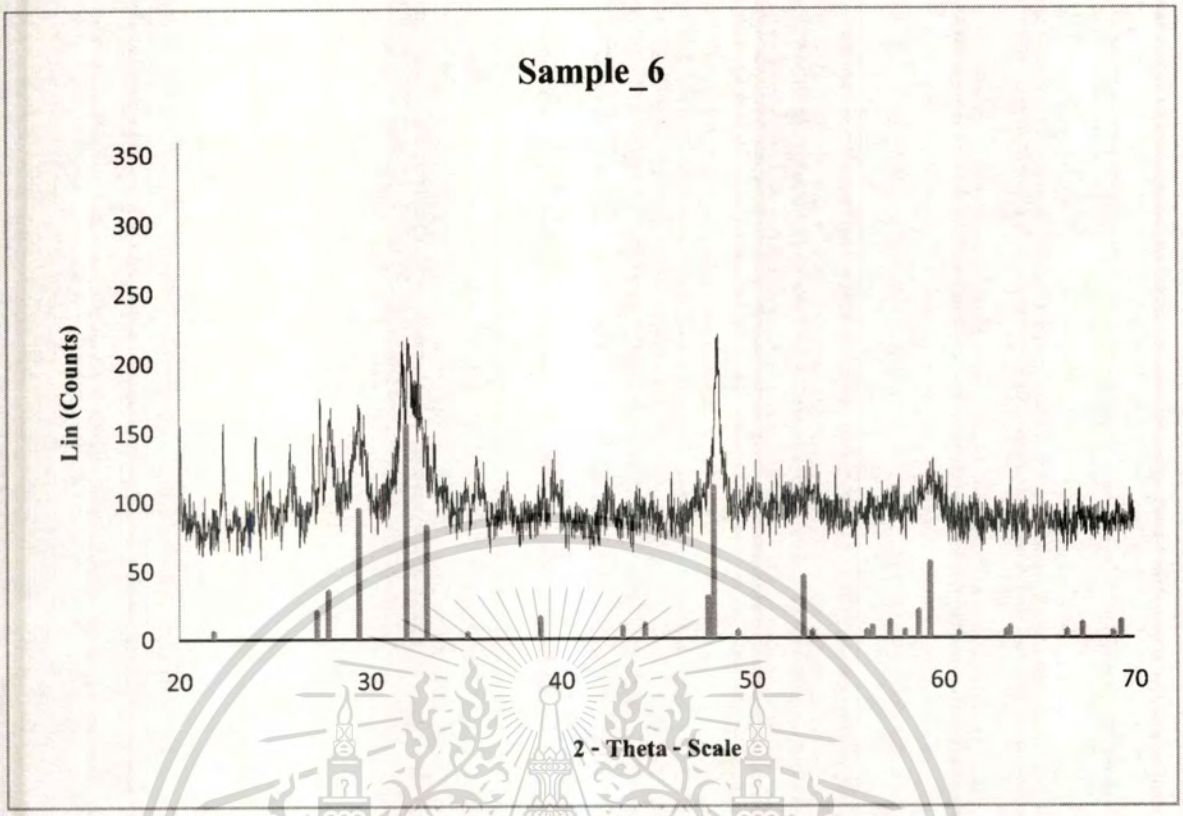

Figure A.5: X-ray Diffraction pattern of sample_6

Sample_6 – File:1XD53_0032_05_sample_6.RAW – Type: 2Th/Th locked – Start: 20.000° - End: 70.000° -Step: 0.020° - Step time: 1.s – Temp.: 25°C (Room) – Time Started: 0 s – 2 – Theta: 20.000° - Theta: 10.000° - Operations: Import

79 - 2321 (C) - Copper Sulfide – CuS – Y: 50.00 % - d x by: 1. – WL: 1.5406 – Hexagonal-a 3.78813 – b 3.78813 – c 16.33307 – alpha 90.000 – beta 90.000 – gamma 120.000 – Primitive – P63/mmc (194) – 6 – 202.978 – I/Ic P

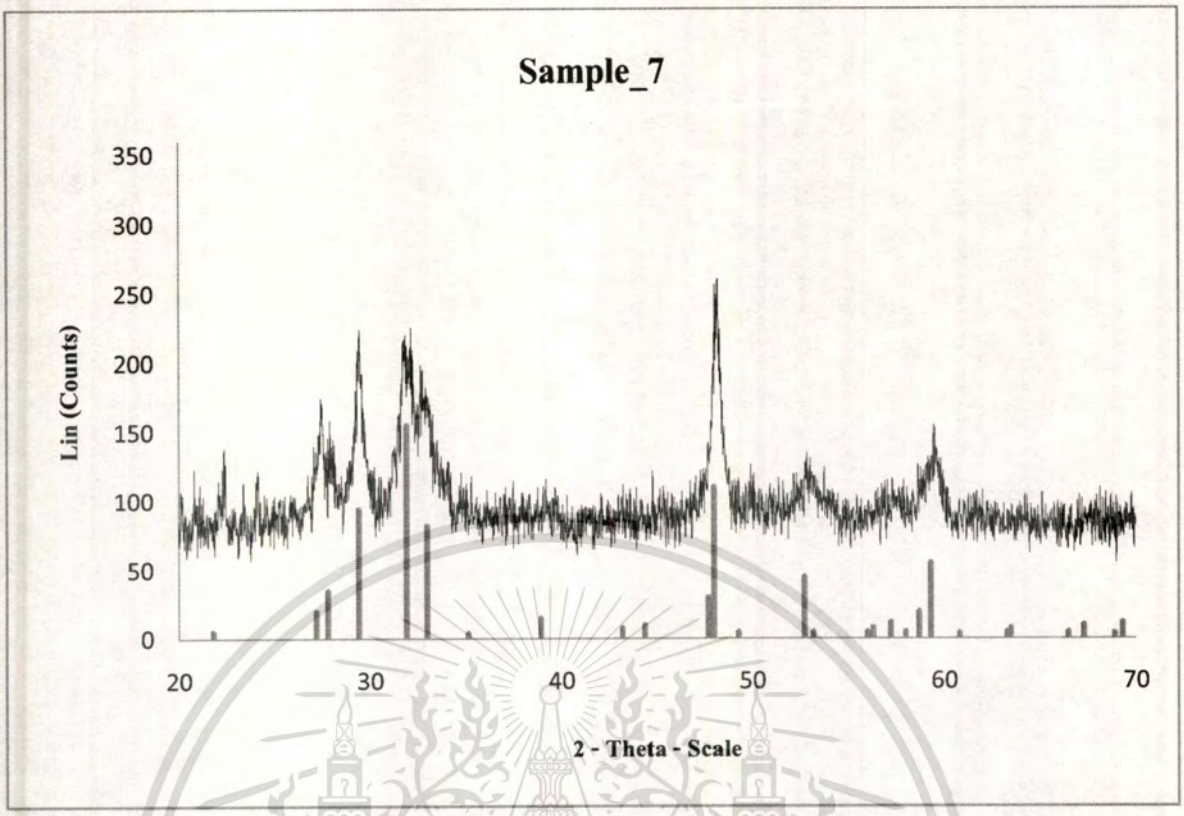

Figure A.6: X-ray Diffraction pattern of sample_7

Sample_7 – File:1XD53_0032_06_sample_7.RAW – Type: 2Th/Th locked – Start: 20.000° - End: 70.000° -Step: 0.020° - Step time: 1.s – Temp.: 25°C (Room) – Time Started: 0 s – 2 – Theta: 20.000° - Theta: 10.000° - Operations: Import

79 - 2321 (C) - Copper Sulfide – CuS – Y: 50.00 % - d x by: 1. – WL: 1.5406 – Hexagonal-a 3.78813 – b 3.78813 – c 16.33307 – alpha 90.000 – beta 90.000 – gamma 120.000 – Primitive – P63/mmc (194) – 6 – 202.978 – I/Ic P

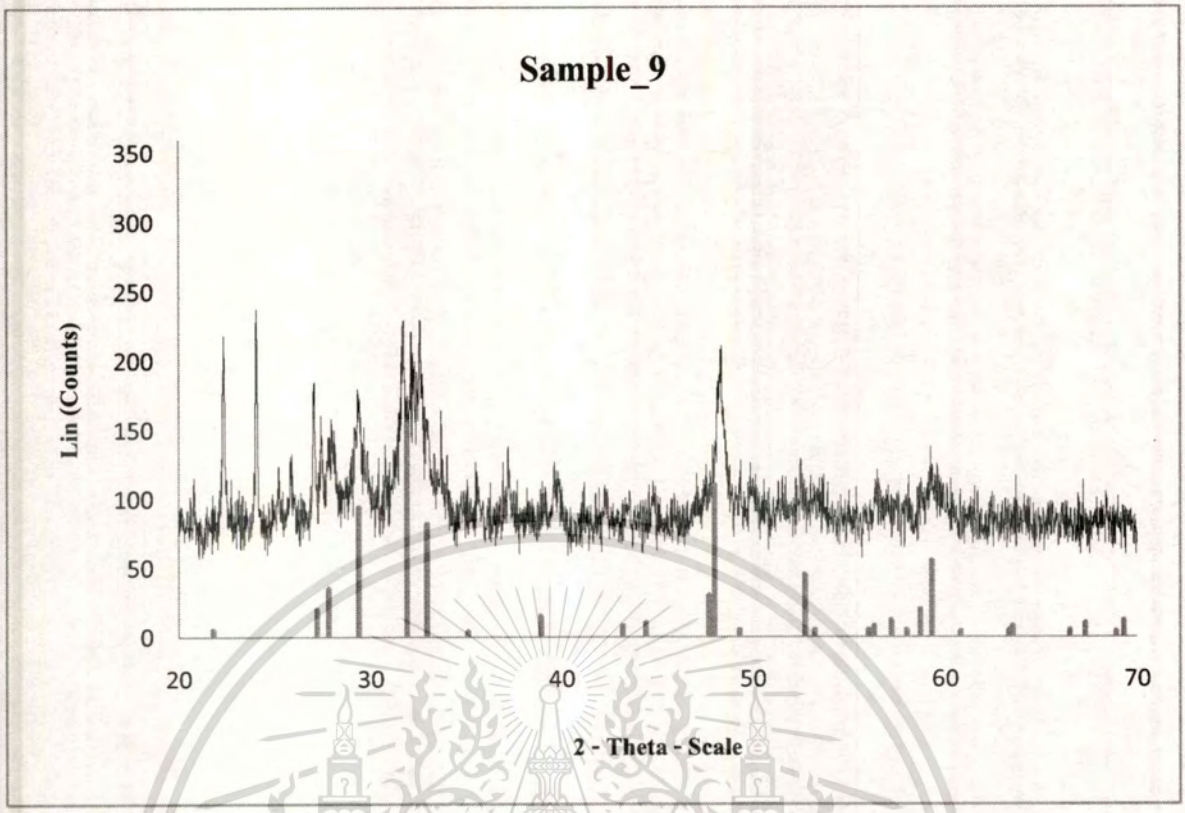

Figure A.7: X-ray Diffraction pattern of sample_9

Sample_9 – File:1XD53_0032_07_sample_9.RAW – Type: 2Th/Th locked – Start: 20.000° - End: 70.000°-Step: 0.020° - Step time: 1.s – Temp.: 25°C (Room) – Time Started: 0 s – 2 – Theta: 20.000° - Theta: 10.000° - Operations: Import

79 - 2321 (C) - Copper Sulfide – CuS – Y: 50.00 % - d x by: 1. – WL: 1.5406 – Hexagonal- a 3.78813 – b 3.78813 – c 16.33307 – alpha 90.000 – beta 90.000 – gamma 120.000 – Primitive – P63/mmc (194) – 6 – 202.978 – I/Ic P

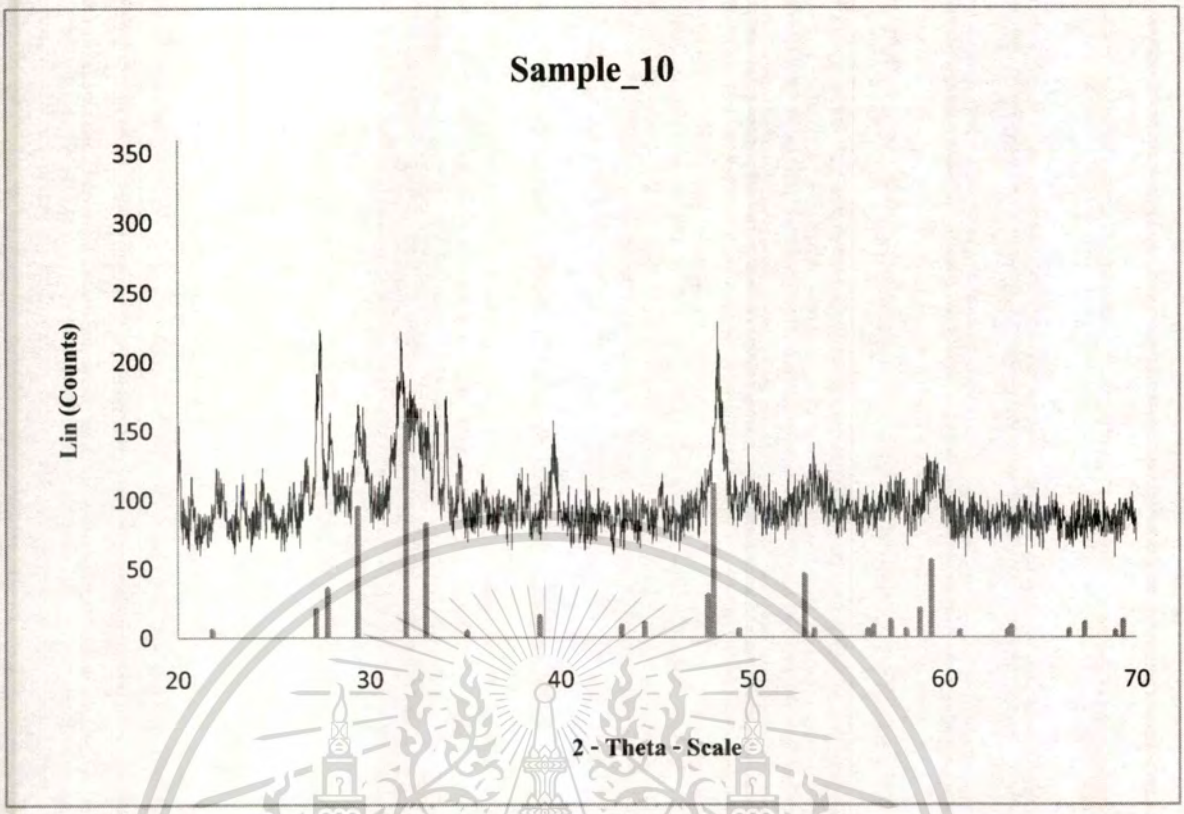

Figure A.8: X-ray Diffraction pattern of sample_10

Sample_10 – File:1XD53_0032_08_sample_10.RAW – Type: 2Th/Th locked – Start: 20.000° - End: 70.000°-Step: 0.020° - Step time: 1.s – Temp.: 25°C (Room) – Time Started: 0 s – 2 – Theta: 20.000° - Theta: 10.000° - Operations: Import

79 - 2321 (C) - Copper Sulfide – CuS – Y: 50.00 % - d x by: 1. – WL: 1.5406 – Hexagonal-a 3.78813 – b 3.78813 – c 16.33307 – alpha 90.000 – beta 90.000 – gamma 120.000 – Primitive – P63/mmc (194) – 6 – 202.978 – I/Ic P

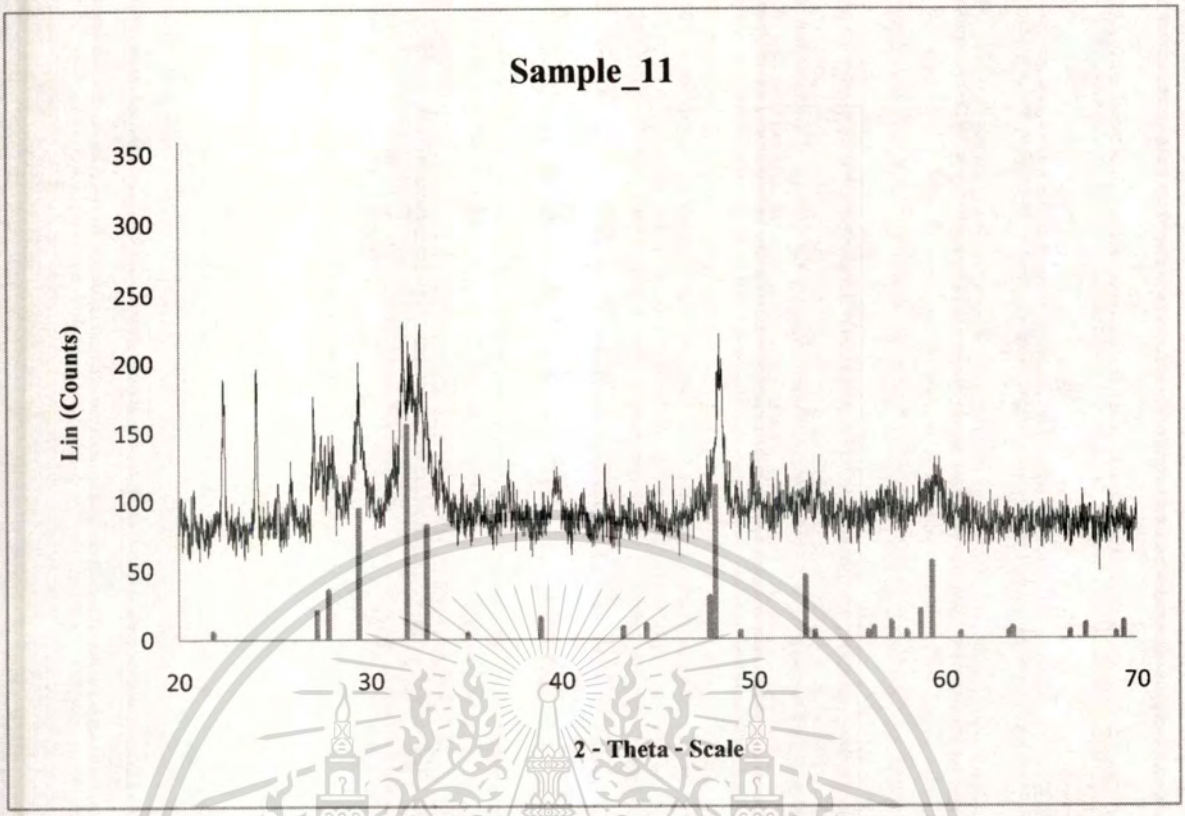

Figure A.9: X-ray Diffraction pattern of sample_11

Sample_11 – File:1XD53_0032_09_sample_11.RAW – Type: 2Th/Th locked – Start: 20.000° - End: 70.000°-Step: 0.020° - Step time: 1.s – Temp.: 25°C (Room) – Time Started: 0 s – 2 – Theta: 20.000° - Theta: 10.000° - Operations: Import

79 - 2321 (C) - Copper Sulfide – CuS – Y: 50.00 % - d x by: 1. – WL: 1.5406 – Hexagonal- a 3.78813 – b 3.78813 – c 16.33307 – alpha 90.000 – beta 90.000 – gamma 120.000 – Primitive – P63/mmc (194) – 6 – 202.978 – I/Ic P

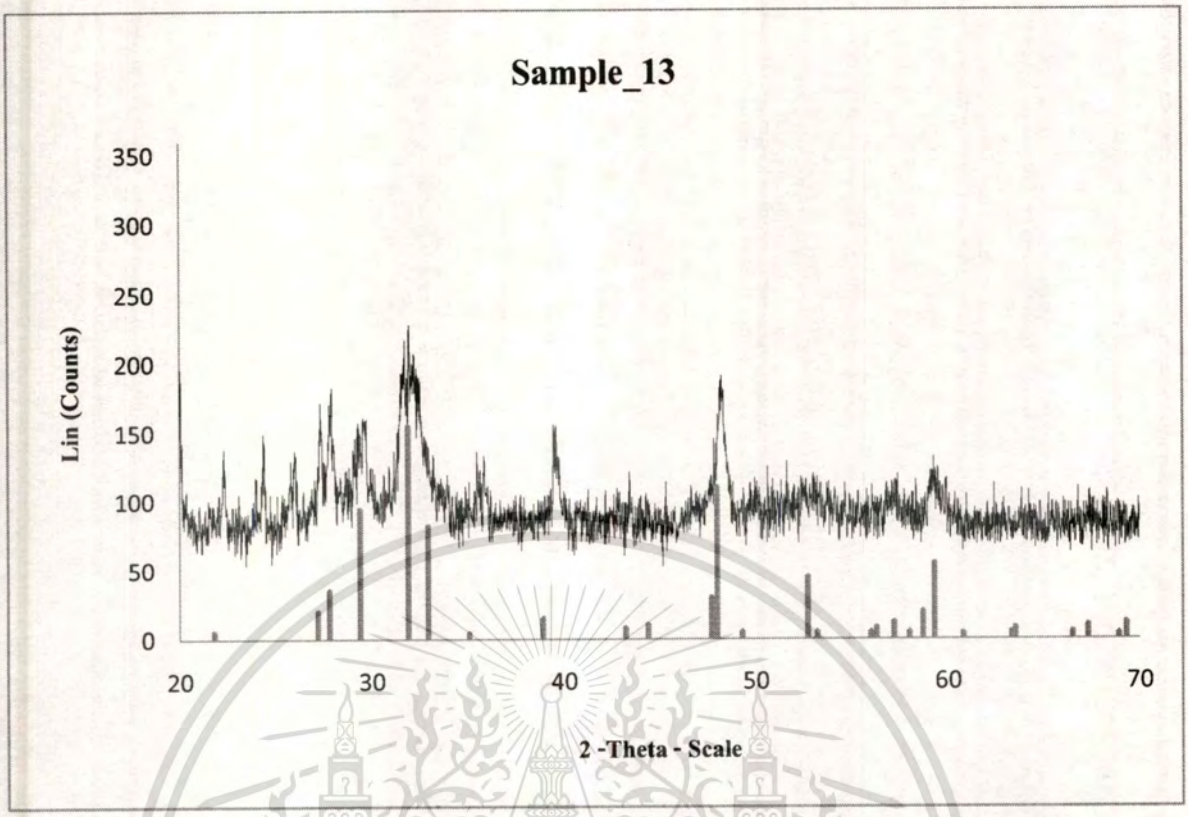

Figure A.10: X-ray Diffraction pattern of sample_13

Sample_13 – File:1XD53_0032_10_sample_13.RAW – Type: 2Th/Th locked – Start: 20.000° - End: 70.000°-Step: 0.020° - Step time: 1.s – Temp.: 25°C (Room) – Time Started: 0 s – 2 – Theta: 20.000° - Theta: 10.000° - Operations: Import

79 - 2321 (C) - Copper Sulfide – CuS – Y: 50.00 % - d x by: 1. – WL: 1.5406 – Hexagonal- a 3.78813 – b 3.78813 – c 16.33307 – alpha 90.000 – beta 90.000 – gamma 120.000 – Primitive – P63/mmc (194) – 6 – 202.978 – I/Ic P

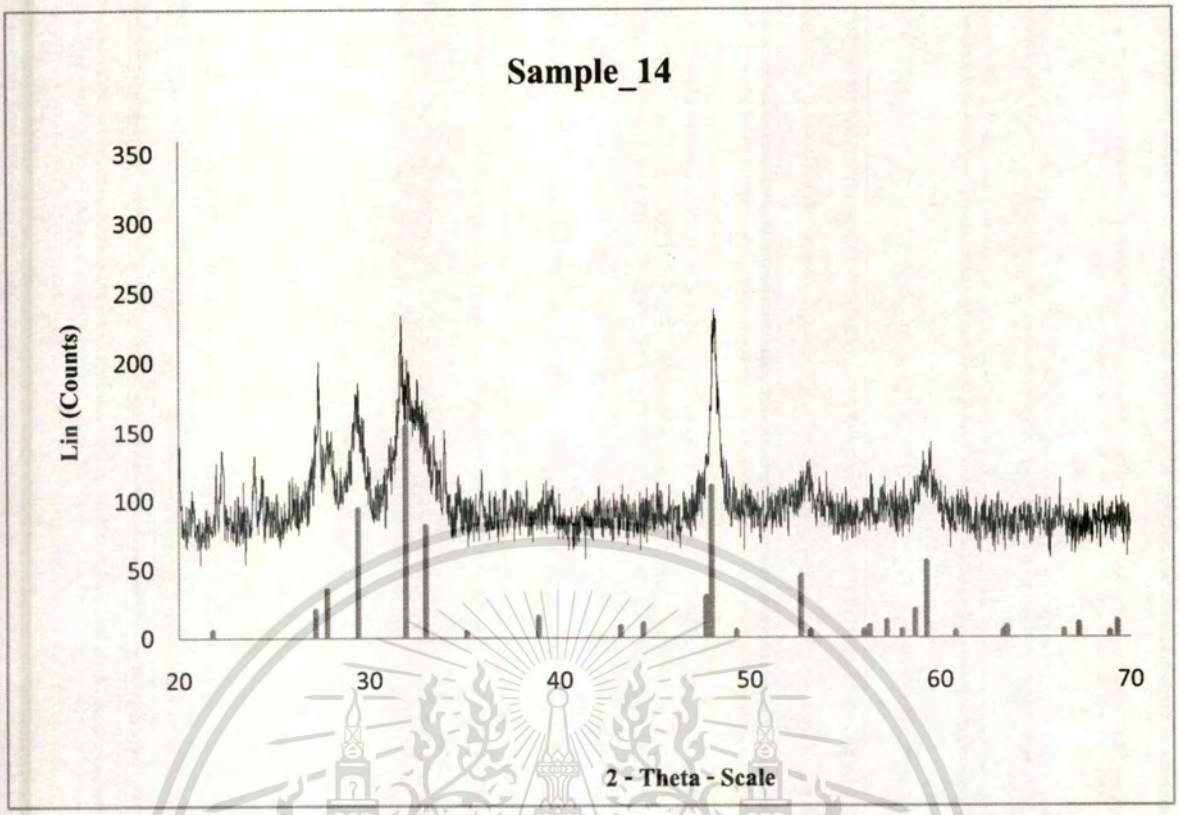

Figure A.11: X-ray Diffraction pattern of sample_14

Sample_14 – File:1XD53_0032_11_sample_14.RAW – Type: 2Th/Th locked – Start: 20.000° - End: 70.000°-Step: 0.020° - Step time: 1.s – Temp.: 25°C (Room) – Time Started: 0 s – 2 – Theta: 20.000° - Theta: 10.000° - Operations: Import

79 - 2321 (C) - Copper Sulfide – CuS – Y: 50.00 % - d x by: 1. – WL: 1.5406 – Hexagonal- a 3.78813 – b 3.78813 – c 16.33307 – alpha 90.000 – beta 90.000 – gamma 120.000 – Primitive – P63/mmc (194) – 6 – 202.978 – I/Ic P

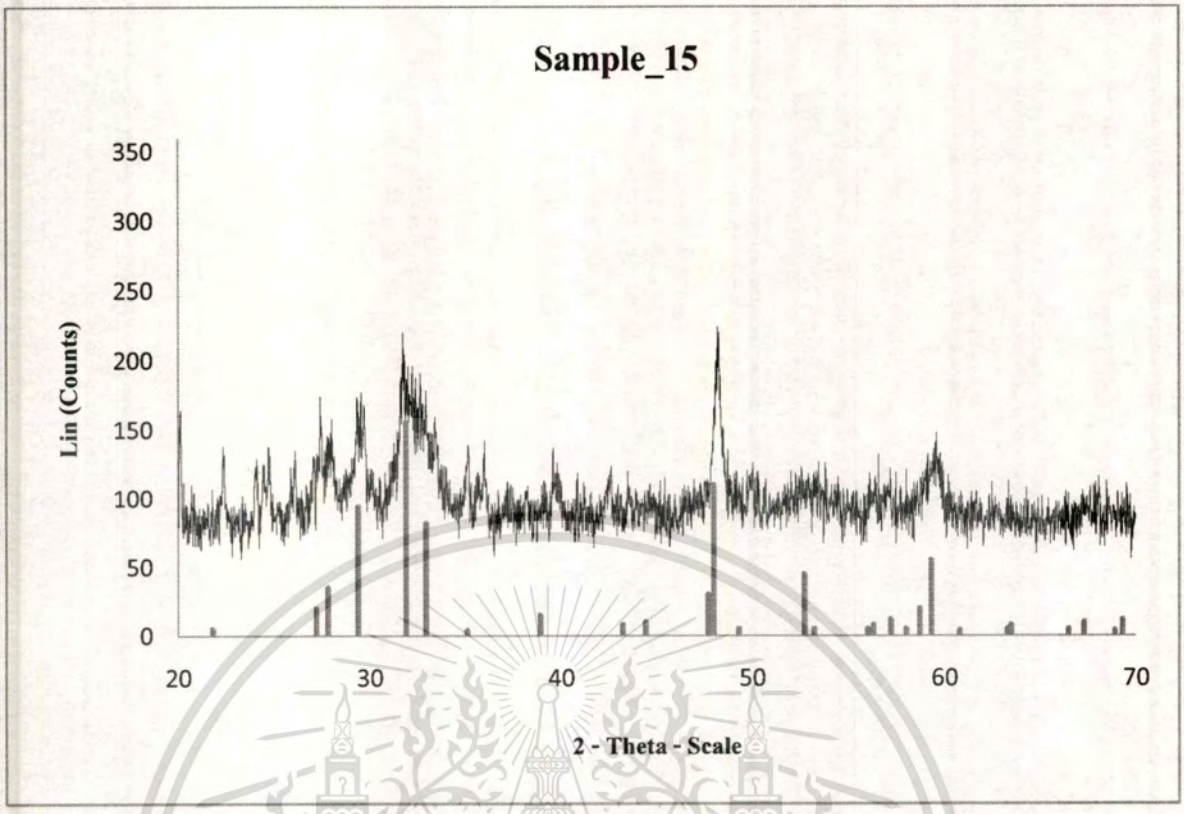

Figure A.12: X-ray Diffraction pattern of sample_15

Sample_15 – File:1XD53_0032_12_sample_15.RAW – Type: 2Th/Th locked – Start: 20.000° - End: 70.000°-Step: 0.020° - Step time: 1.s – Temp.: 25°C (Room) – Time Started: 0 s – 2 – Theta: 20.000° - Theta: 10.000° - Operations: Import

79 - 2321 (C) - Copper Sulfide – CuS – Y: 50.00 % - d x by: 1. – WL: 1.5406 – Hexagonal- a 3.78813 – b 3.78813 – c 16.33307 – alpha 90.000 – beta 90.000 – gamma 120.000 – Primitive – P63/mmc (194) – 6 – 202.978 – I/Ic P

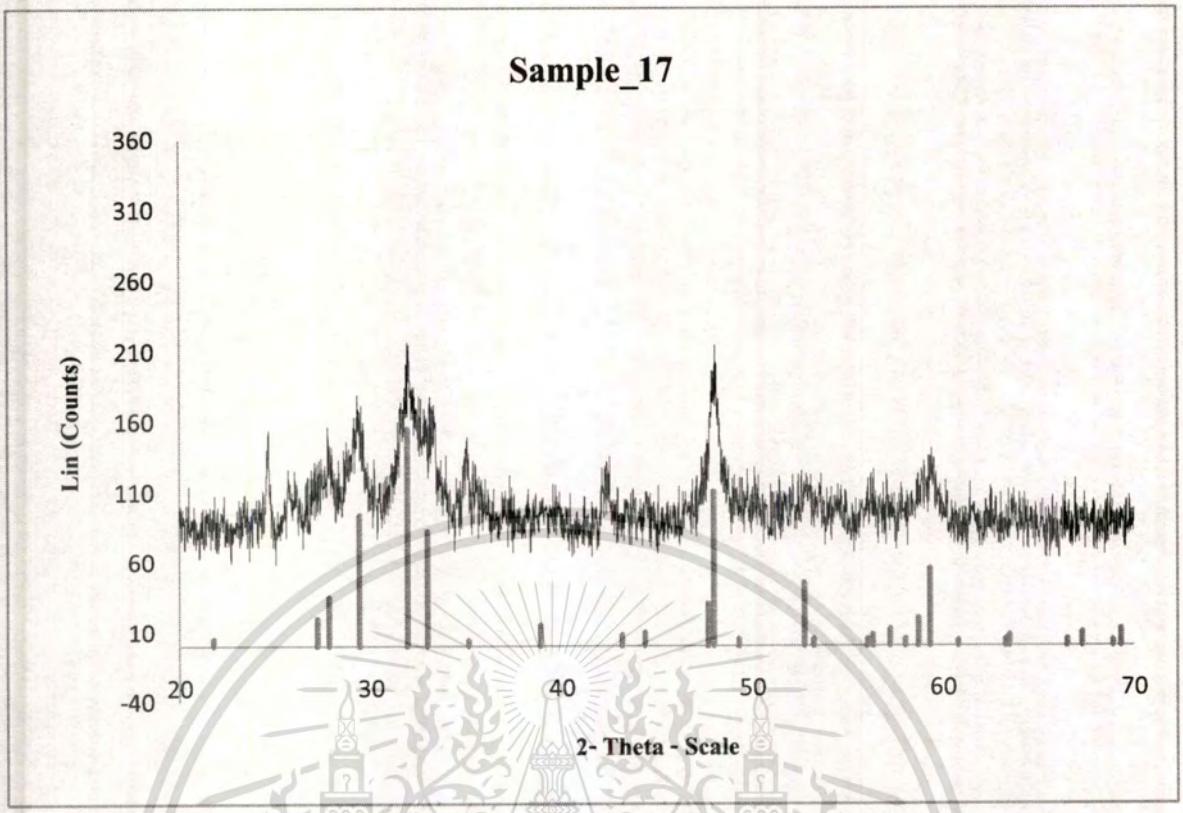

Figure A.13: X-ray Diffraction pattern of sample_17

Sample_17 – File:3XD53_0054_01_sample_17.RAW – Type: 2Th/Th locked – Start: 20.000° - End: 70.000°-Step: 0.020° - Step time: 1.s – Temp.: 25°C (Room) – Time Started: 0 s – 2 – Theta: 20.000° - Theta: 10.000° - Operations: Import

79 - 2321 (C) - Copper Sulfide – CuS – Y: 50.00 % - d x by: 1. – WL: 1.5406 – Hexagonal- a 3.78813 – b 3.78813 – c 16.33307 – alpha 90.000 – beta 90.000 – gamma 120.000 – Primitive – P63/mmc (194) – 6 – 202.978 – I/Ic P

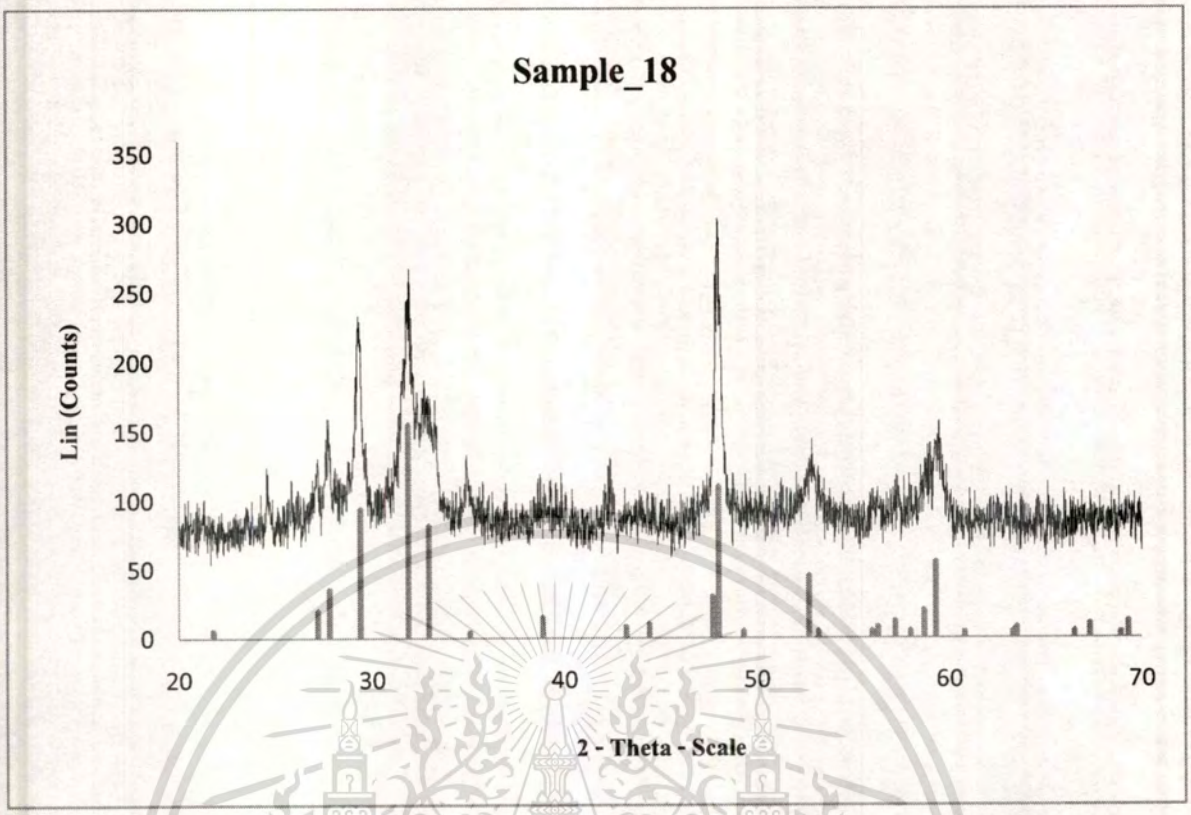

Figure A.14: X-ray Diffraction pattern of sample_18

Sample_18 – File:3XD53_0054_02_sample_18.RAW – Type: 2Th/Th locked – Start: 20.000° - End: 70.000°-Step: 0.020° - Step time: 1 s – Temp.: 25°C (Room) – Time Started: 0 s – 2 – Theta: 20.000° - Theta: 10.000° - Operations: Import

79 - 2321 (C) - Copper Sulfide – CuS – Y: 50.00 % - d x by: 1. – WL: 1.5406 – Hexagonal- a 3.78813 – b 3.78813 – c 16.33307 – alpha 90.000 – beta 90.000 – gamma 120.000 – Primitive – P63/mmc (194) – 6 – 202.978 – I/Ic P

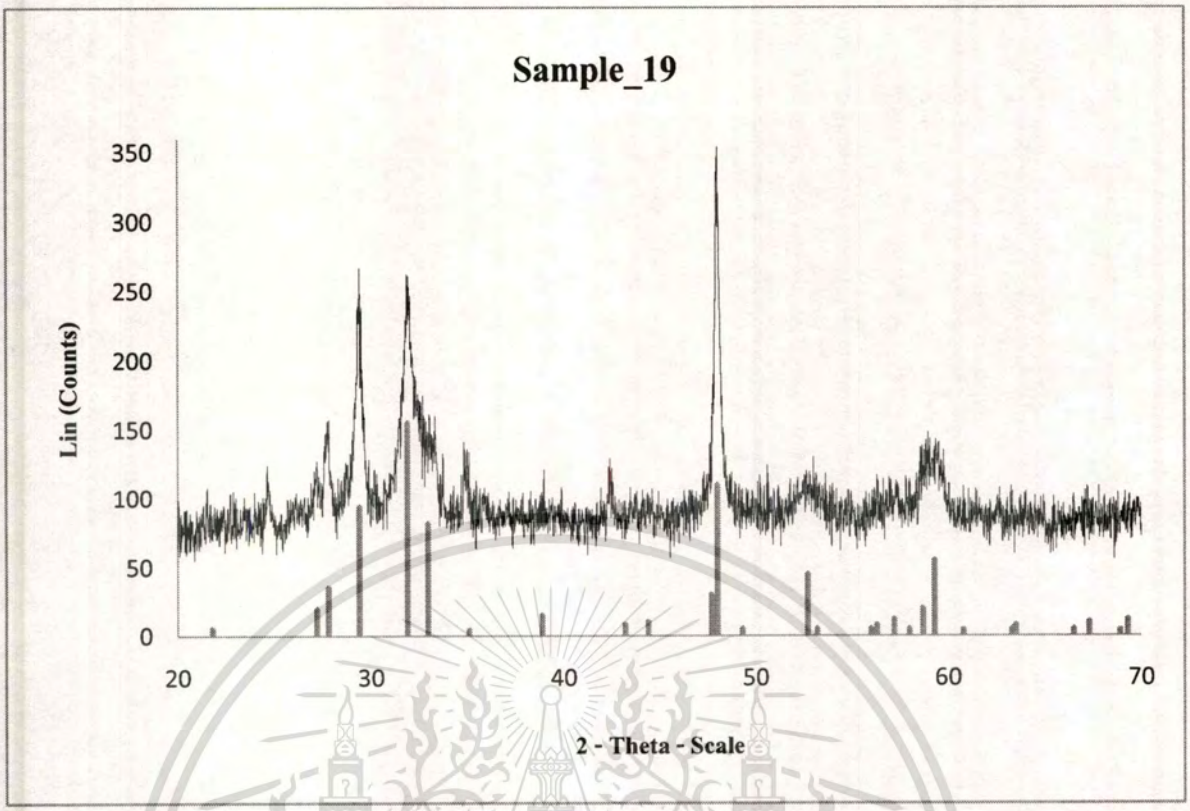

Figure A.15: X-ray Diffraction pattern of sample_19

Sample_19 – File:3XD53_0054_03_sample_19.RAW – Type: 2Th/Th locked – Start: 20.000° - End: 70.000°-Step: 0.020° - Step time: 1.s – Temp.: 25°C (Room) – Time Started: 0 s – 2 – Theta: 20.000° - Theta: 10.000° - Operations: Import

79 - 2321 (C) - Copper Sulfide – CuS – Y: 50.00 % - d x by: 1. – WL: 1.5406 – Hexagonal- a 3.78813 – b 3.78813 – c 16.33307 – alpha 90.000 – beta 90.000 – gamma 120.000 – Primitive – P63/mmc (194) – 6 – 202.978 – I/Ic P

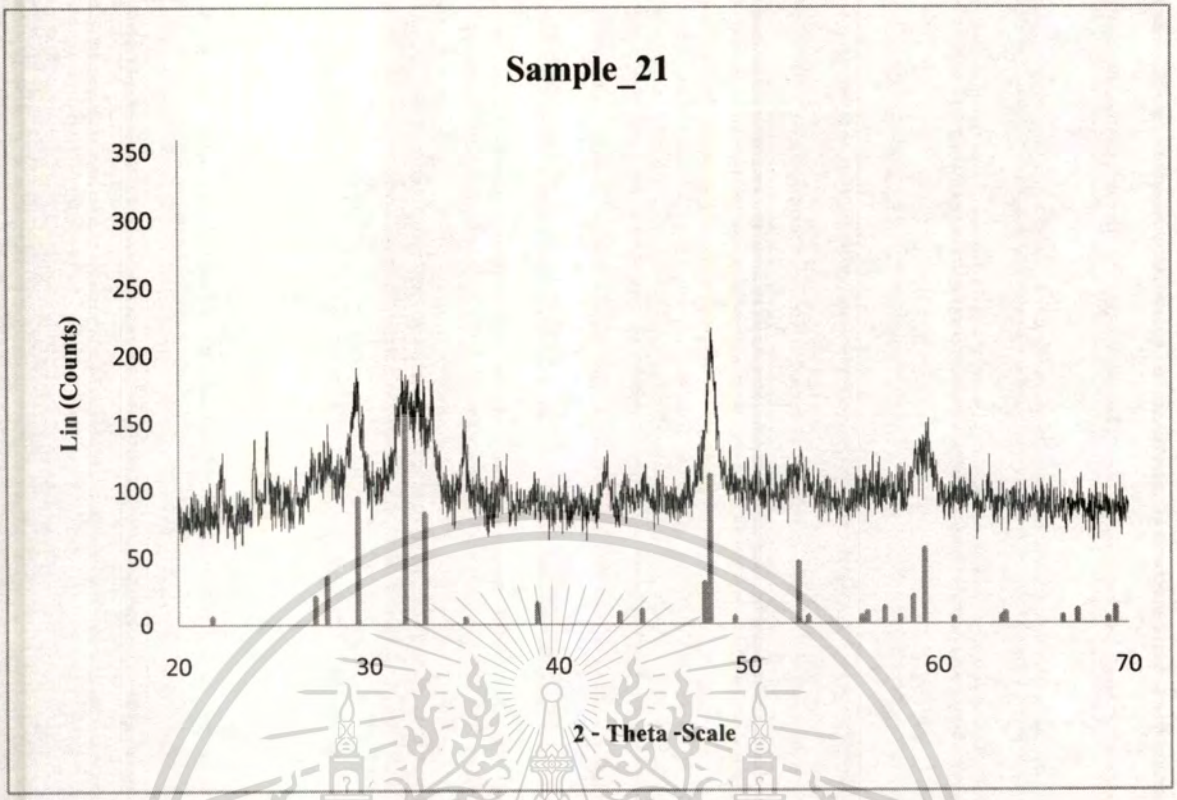

Figure A.16: X-ray Diffraction pattern of sample_21

Sample_21 – File:3XD53_0054_04_sample_21.RAW – Type: 2Th/Th locked – Start: 20.000° - End: 70.000°-Step: 0.020° - Step time: 1.s – Temp.: 25°C (Room) – Time Started: 0 s – 2 – Theta: 20.000° - Theta: 10.000° - Operations: Import

79 - 2321 (C) - Copper Sulfide – CuS – Y: 50.00 % - d x by: 1. – WL: 1.5406 – Hexagonal- a 3.78813 – b 3.78813 – c 16.33307 – alpha 90.000 – beta 90.000 – gamma 120.000 – Primitive – P63/mmc (194) – 6 – 202.978 – I/Ic P

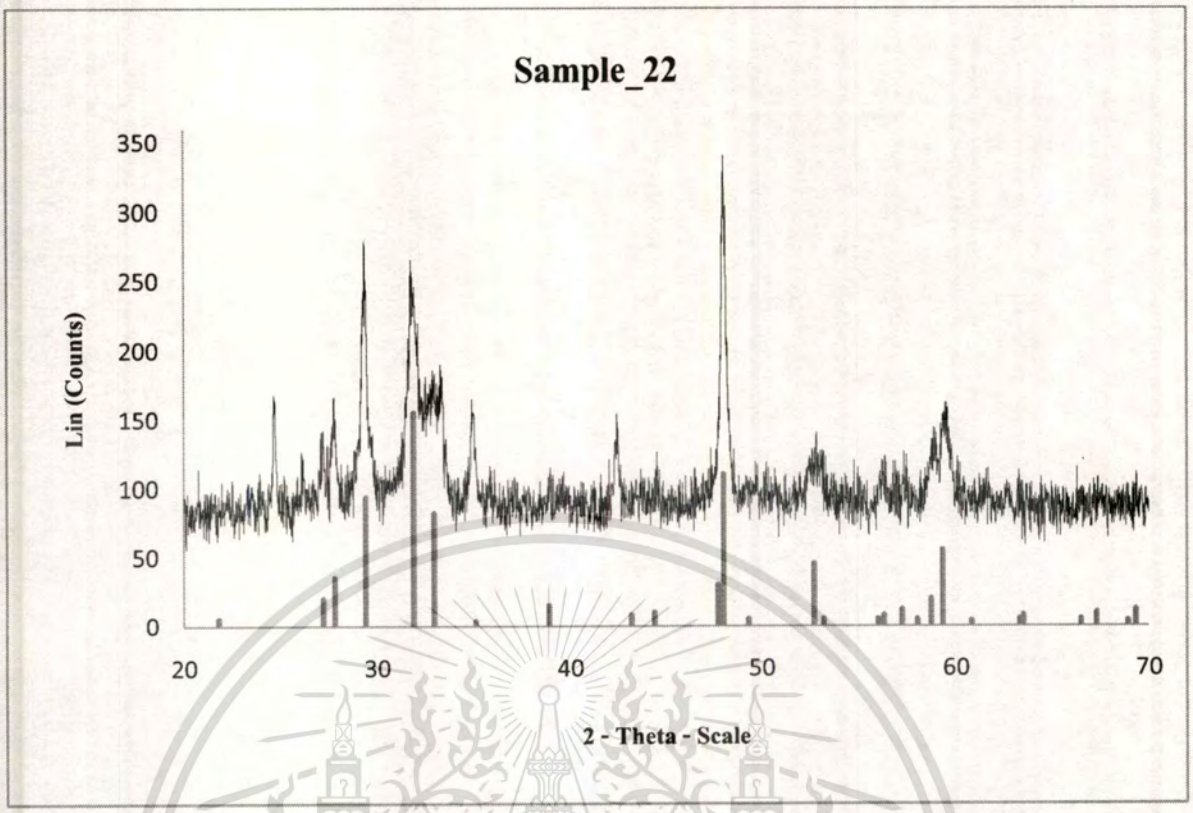

Figure A.17: X-ray Diffraction pattern of sample_22

Sample_22 – File:3XD53_0054_05_sample_22.RAW – Type: 2Th/Th locked – Start: 20.000° - End: 70.000°-Step: 0.020° - Step time: 1.s – Temp.: 25°C (Room) – Time Started: 0 s – 2 – Theta: 20.000° - Theta: 10.000° - Operations: Import

79 - 2321 (C) - Copper Sulfide – CuS – Y: 50.00 % - d x by: 1. – WL: 1.5406 – Hexagonal- a 3.78813 – b 3.78813 – c 16.33307 – alpha 90.000 – beta 90.000 – gamma 120.000 – Primitive – P63/mmc (194) – 6 – 202.978 – I/Ic P

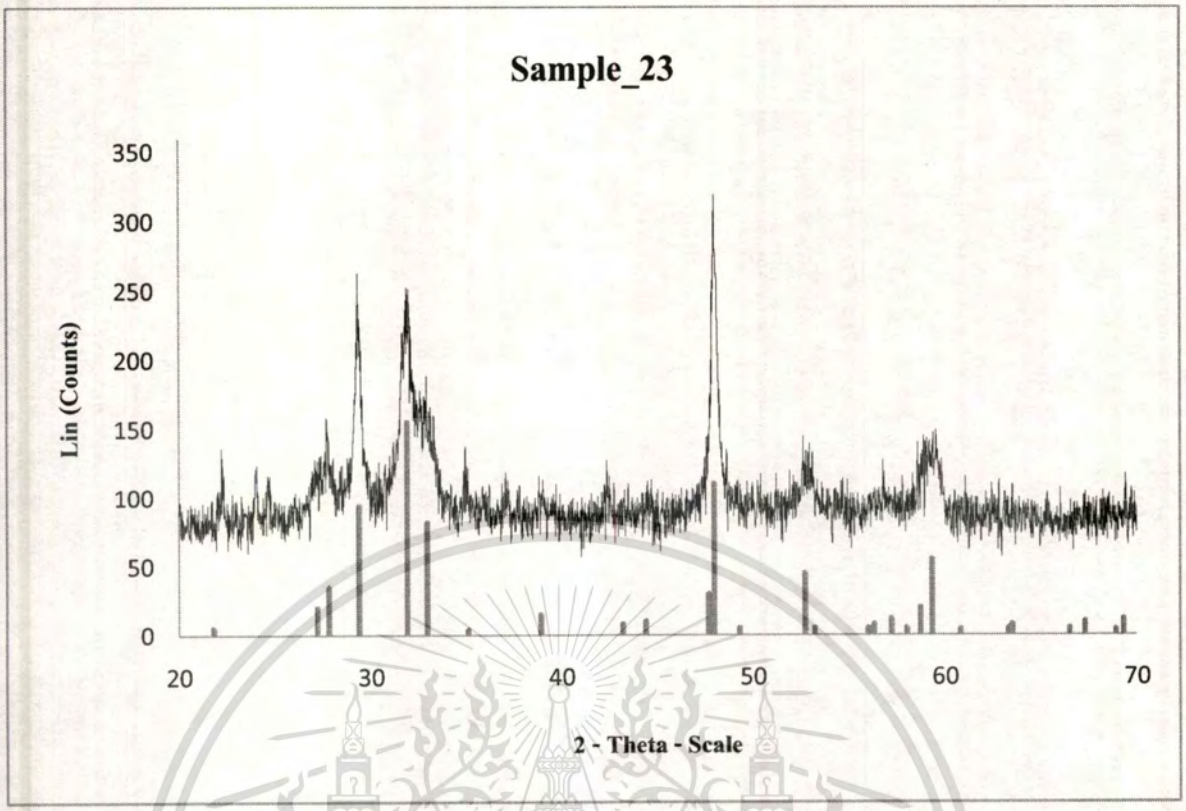

Figure A.18: X-ray Diffraction pattern of sample_23

Sample_23 – File:3XD53_0054_06_sample_23.RAW – Type: 2Th/Th locked – Start: 20.000° - End: 70.000°-Step: 0.020° - Step time: 1.s – Temp.: 25°C (Room) – Time Started: 0 s – 2 – Theta: 20.000° - Theta: 10.000° - Operations: Import

79 - 2321 (C) - Copper Sulfide – CuS – Y: 50.00 % - d x by: 1. – WL: 1.5406 – Hexagonal- a 3.78813 – b 3.78813 – c 16.33307 – alpha 90.000 – beta 90.000 – gamma 120.000 – Primitive – P63/mmc (194) – 6 – 202.978 – I/Ic P

A.4 SEM Images

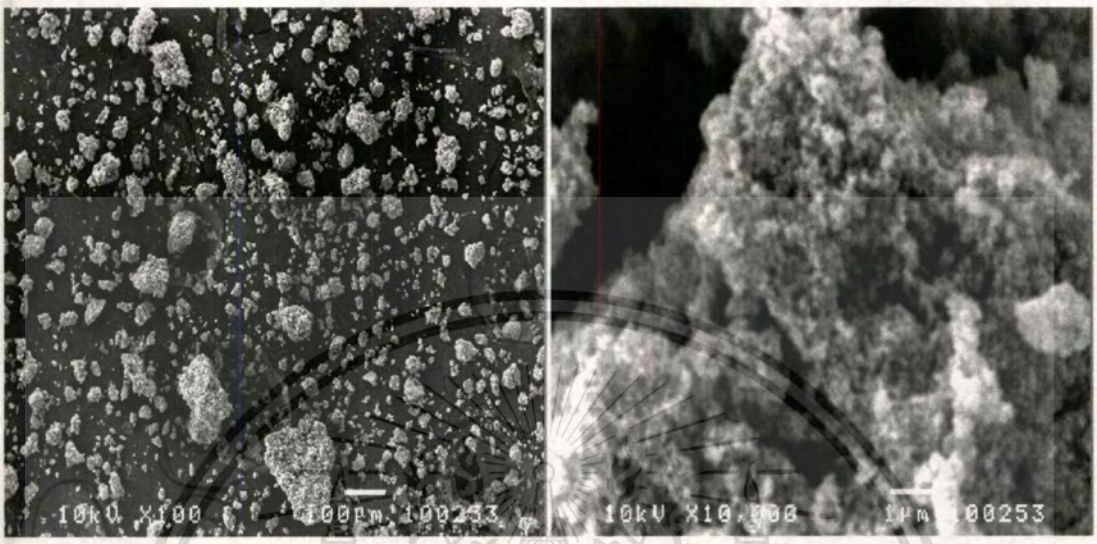

(a) (b)

Figure A.19: (a) and (b) show SEM image of sample 14a at 100x and 10,000x

A.5 TEM Images

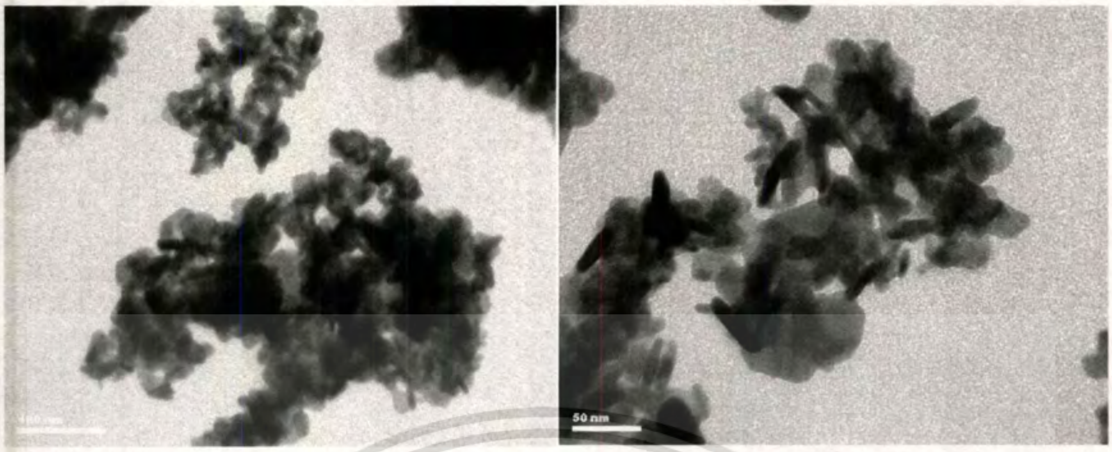

(a) (b)

Figure A.20: TEM image of sample 6a (a) 100 nm in scale and (b) 50 nm in scale

(a) (b)

Figure A.21: TEM image of sample 10a (a) 100 nm in scale and (b) 50 nm in scale

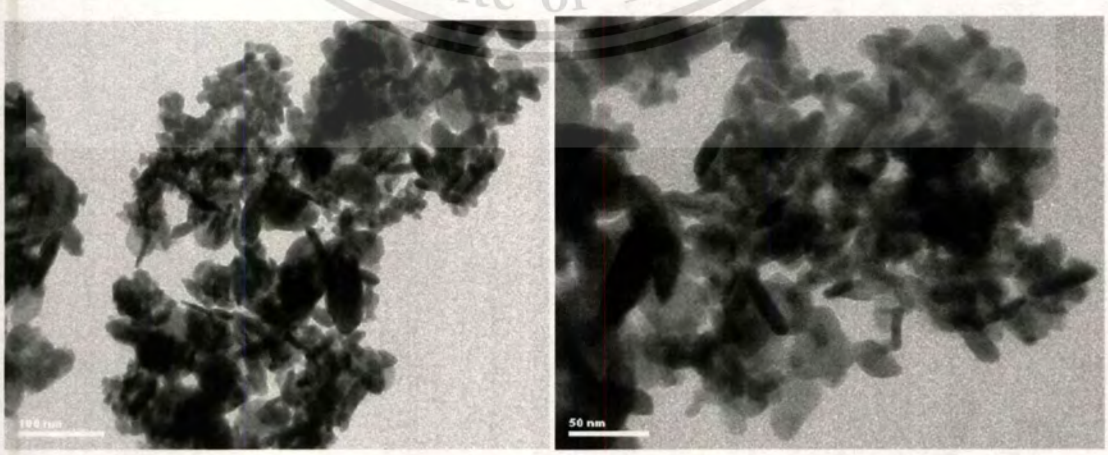

(a) (b)

Figure A.22: TEM image of sample 13a (a) 100 nm in scale and (b) 50 nm in scale

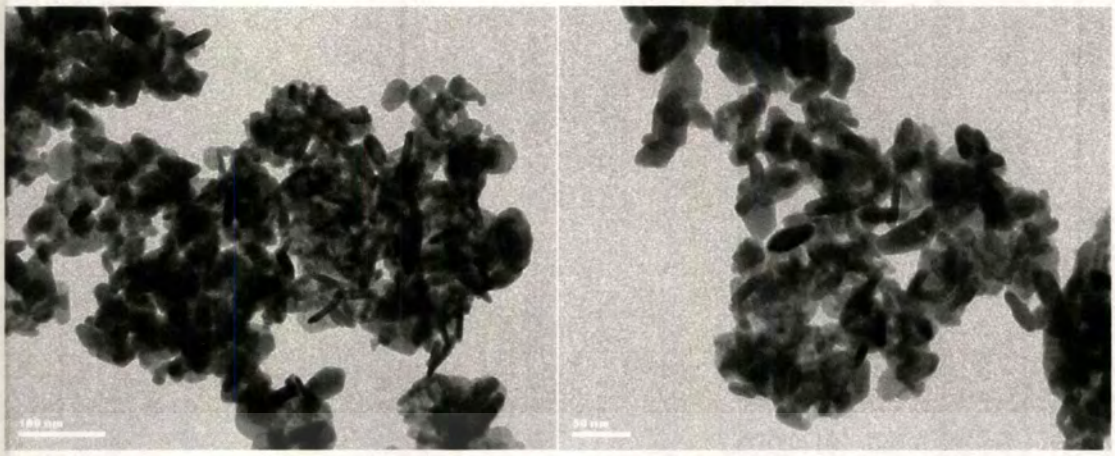

(a) (b)

Figure A.23: TEM image of sample 14a (a) 100 nm in scale and (b) 50 nm in scale

(a) (b)

Figure A.24: TEM image of sample 15a (a) 100 nm in scale and (b) 50 nm in scale

(a) (b)

Figure A.25: TEM image of sample 22a (a) 100 nm in scale and (b) 50 nm in scale

Appendix B

Calculation

B.1 Calculation of Percent Yield

$$\text{Percentage Yield} = \frac{\text{mass of Actual Yield}}{\text{mass of Theoretical Yield}} \times 100$$

Theoretical Yield

Mass = No. of moles × molar mass

= (0.025moles) × (95.62g/mole)

= 2.39g

Example: from the experiment data A.1sample 7

$$\text{Percentage Yield} = \frac{2.3801}{2.39} \times 100$$

= 99.59 %

The result of percentage yield of others sample shown in chapter 4, Table 4.3

B.2 Calculation of Particle Size

The crystallite size was calculated from the half-height width of the diffraction peak of XRD pattern using the Debye - Scherrer equation.

From Scherrer equation:

$$\text{Particle size} = \frac{K\lambda}{\beta \times \cos\theta}$$

K = constant dependent on crystallite shape, K = 0.9 for unknown shape

λ = wavelength of x-rays of Cu K_α, λ = 0.1542nm

β = FWHM (full width at half maximum of the reflection peak that has the same maximum intensity in the diffraction pattern)

θ = diffraction angle of x-rays

Example: Calculation of particle size of sample 14

Where; λ = 0.1542nm

K = 0.9

Find; θ = 24.025° (from the figure B.1)

= (24.025 × π) ÷ 180 ; π = 22/7

= 0.419484 radian

cosθ = 0.913299

From figure B.1;

2θ high (°) = 48.4

2θ low (°) = 47.9

FWHM (°) = 48.4 – 47.9 = 0.5

FWHM = (0.5 × π) ÷ 180 ; π = 22/7

= 0.00873 radian

$$\text{The particle size} = \frac{(0.9)\times(1.542)}{(0.00873)\times(0.913299)}$$

= 17.4057 nm

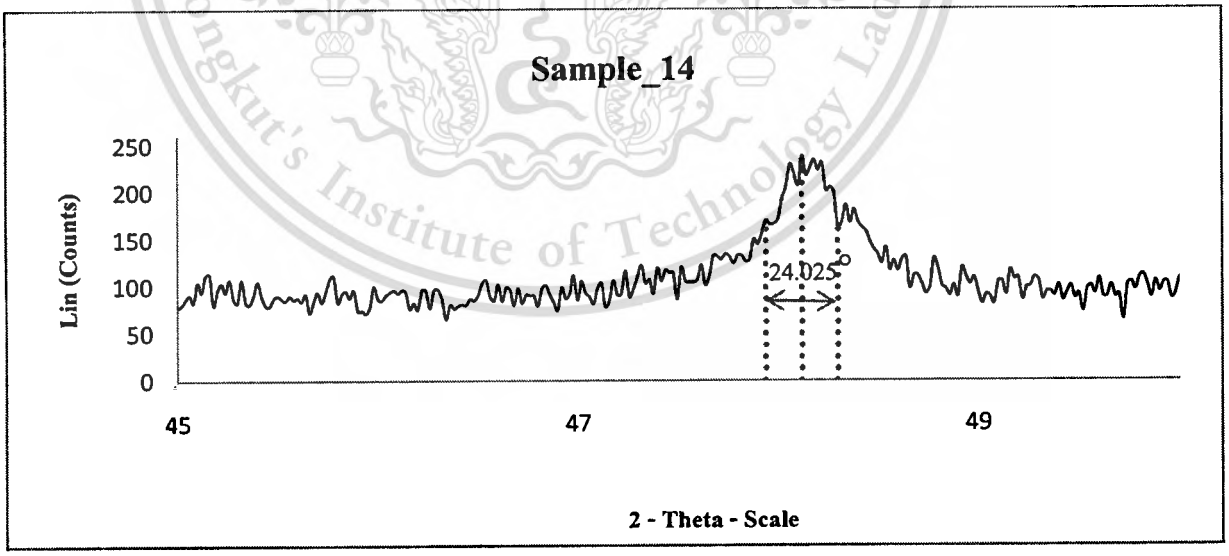

Figure B.1: The diffraction peak of sample 14 for calculation of particle size

The result of particle size of others sample shown in chapter 4, Table 4.2